Nonequilibrium Green Functions Analysis of Time Reversal Symmetry in Hubbard Clusters

M. J. Scharnke

Bachelor thesis

Institut für Theoretische Physik und Astrophysik
Christian–Albrechts–Universität zu Kiel
July 28, 2016

First examiner:	Prof. Dr. Michael Bonitz
Second examiner:	Dr. Sebastian Bauch

Abstract

Time reversal symmetry is a fundamental property of many quantum mechanical systems. The relation between statistical physics and time reversal is subtle and not all statistical theories conserve this particular symmetry. In this thesis it is shown analytically that the governing equations of the nonequilibrium Green functions formalism as well as many common approximations (Hartree–Fock, second Born and T-matrix approximations of the selfenergy) are time reversal invariant. These results are then checked numerically in small, one-dimensional Hubbard clusters. The stability of time reversal invariance is analysed by perturbing the system slightly during time reversal.

Zusammenfassung

Zeitumkehrsymmetrie ist eine fundamentale Eigenschaft vieler quantenmechanischer Systeme. Der Zusammenhang zwischen statistischer Physik und Zeitumkehr ist schwierig, und nicht alle statistischen Theorien erhalten Zeitumkehrsymmetrie. In dieser Arbeit wird analytisch gezeigt, dass die Gleichungen der Nichtgleichgewichtsgreenfunktionstheorie vollständig invariant bezüglich Zeitumkehr sind, ebenso wie viele der häufig verwendeten Näherungen (die Hartree–Fock-Näherung, die zweite Born'sche Näherung und die T-Matrix-Näherung der Selbstenergie). Die theoretischen Ergebnisse werden anschließend numerisch auf ein einfaches Fallbeispiel kleiner, eindimensionaler Hubbardcluster angewandt. Die Stabilität der Zeitumkehrinvarianz wird untersucht, indem das System während der Umkehr leicht gestört wird.

Contents

1 Introduction

Time reversal symmetry (or T-symmetry) has for a long time been thought to be one of the fundamental symmetries of the universe[1, 2, 3]. It is known today that there are instances when time reversal symmetry is broken (for example the electroweak decay of the kaon K^+[1, 2, 4]) and that the fundamental symmetry is CPT-symmetry (charge, parity and time reversal): For any physically allowed process, the CPT-reversed process must also be possible, i.e., the process where matter has been replaced by antimatter, where all vectors have been replaced by their mirror images, and where time has been replaced by its negative[1, 3]. However, in most cases, CP- and T-symmetry are conserved independently of one another.

T-symmetry, besides being a fundamental property of many (though not all) quantum mechanical systems, is also useful from the point of view of numerical testing[5, 6, 7]. Letting a system propagate in time according to some algorithm and then letting it propagate backwards in time according to the same algorithm yields a predictable result—the initial state—with which to compare the outcome. Of course, this only works if the equations on which the algorithm is based are themselves symmetric with respect to time reversal.

The purpose of this thesis is to analyse the T-symmetry properties of the Green functions formalism.

The theory of nonequilibrium Green functions is a statistical description of quantum many-particle systems which has gained much importance over the last two decades, mainly due to the ever increasing computing power[8, 9, 10]. It allows the ab initio calculation of systems of arbitrary dimension and considerable size[11]. Amongst its applications are photoionization processes[12], the dynamics of few-electron systems[13, 14] and the dynamics of strongly correlated fermionic and bosonic systems in traps or optical lattices [15].

Since not all statistical theories are time reversal invariant (one well-known counterexample being the Boltzmann theory of classical statistical mechanics[8]) it is worth considering whether the Green functions formalism is.

In sections 2.1 and 2.2 the Green functions formalism as well as some aspects of second quantization that are necessary for its understanding are introduced.

In section 2.3 the terminology and concepts of time reversal symmetry, in particular in quantum mechanics, are introduced and then applied to the equations of motion of nonequilibrium Green functions theory: the Martin–Schwinger hierarchy and the Kadanoff–Baym equations (which formally close the first hierarchy equations by introduction of the selfenergy). It is shown that these exact equations are time reversal invariant, as well as all the approximations to the selfenergy which have been considered in this thesis: the Hartree–Fock, second Born and T-matrix selfenergies. A sufficient condition for the time reversibility of the selfenergy is derived. Finally, it is shown that reversing time in the Kadanoff–Baym equations (as well as in exact quantum mechanics) is formally equivalent to changing the sign of the Hamiltonian.

In section 3 the Hubbard model is briefly introduced. The Hubbard model is an idealized solid-state model that describes electrons in a fixed solid state lattice, taking into account the quantum mechanical motion of the electrons in terms of tunnelling from site to site, and short-ranged repulsive (Coulomb) interaction between the electrons[16].

In section 4 these theoretical results are applied to and tested numerically in a small model system, a one-dimensional, four-site Hubbard chain. Additionally, the stability of this system with respect to perturbations to the Hamiltonian during time reversal is tested.

2 Theory

In the first part of this section, all tools that are needed for understanding the theoretical concepts necessary for this thesis are introduced. These are, to begin with, the basic principles of second quantization and nonequilibrium Green functions theory. Nonequilibrium Green functions provide an exact description of many-particle systems. Their dynamics is described by a hierarchy of coupled integro-differential equations. In practice, the first-order hierarchy equations are formally closed by intoduction of a quantity called the selfenergy Σ. This quantity, as well as several methods of its approximation, are presented. Furthermore, the concept of time reversal symmetry as it applies to this thesis is discussed.

In the second part of this section it is shown that the exact equations of the Green functions theory as well as all the approximations that have been considered in this thesis are time reversal symmetric. A sufficient criterion for the numerical reversibility of the selfenergy approximations is derived, considering only the functional relation between the selfenergy and the single-particle Green function. Finally it is shown that in Green functions theory, reversing time is formally equivalent to reversing the sign of the Hamiltonian, similar to the case of the Schrödinger equation.

2.1 Second Quantization

Second quantization is a description of quantum mechanical systems in which the state of a system is represented by occupation numbers of the underlying single-particle orbitals. Once the orbitals are known, the occupation numbers contain the entire information of the state of the system. That state can be written as

$$|\psi\rangle := |n_1,\, n_2\,...\rangle\;, \tag{2.1}$$

where n_i is the occupation number of the i-th orbital. It is therefore possible for any operator acting on that system to be expressed as a combination of two operators: The creation operator $\hat{c}_i^\dagger$ that increases the occupation number of the i-th orbital by one, and the annihilation operator $\hat{c}_i$ that reduces that number by one in the following way:

$$\hat{c}_i^\dagger|n_1,\, n_2\,...,\, n_i,\, ...\rangle = (\pm 1)^\alpha \sqrt{n_i+1}\,|n_1,\, n_2\,...,\, n_i{+}1,\, ...\rangle \begin{cases} 1 & \text{for bosons} \\ \delta_{n_i,0} & \text{for fermions} \end{cases}\;, \tag{2.2}$$

$$\hat{c}_i|n_1,\,n_2\,...,\,n_i,\,...\rangle = (\pm 1)^{\alpha}\sqrt{n_i}\,|n_1,\,n_2\,...,\,n_i{-}1,\,...\rangle \begin{cases} 1-\delta_{n_i,0} & \text{for bosons} \\ \delta_{n_i,1} & \text{for fermions} \end{cases} \quad , \tag{2.3}$$

where $\alpha = \sum_{j=1}^{i-1} n_j$.
This yields the commutation (anticommutation) relations for bosons (fermions),

$$\left[\hat{c}_i,\,\hat{c}_j^{\dagger}\right]_{-(+)} = \delta_{ij} \qquad \text{and} \tag{2.4}$$

$$\left[\hat{c}_i,\,\hat{c}_j\right]_{-(+)} = \left[\hat{c}_i^{\dagger},\,\hat{c}_j^{\dagger}\right]_{-(+)} = 0\;. \tag{2.5}$$

From these relations follows one of the main advantages of this formulation, which is the fact that it inherently contains the symmetry and antisymmetry of the bosonic and fermionic wave functions.
The representation of single and multiple particle operators as a combination of creation and annihilation operators follows directly from their matrix representations. Let $\hat{b}_1$ be a single-particle operator. Its representation in second quantization is then:

$$\hat{B}_1 = \sum_{i,j=1}^{M} \underbrace{\langle i|\,\hat{b}_1\,|j\rangle}_{b_{ij}}\,\hat{c}_i^{\dagger}\,\hat{c}_j\;, \tag{2.6}$$

where M is the number of single particle orbitals and can be infinity. Similarly, a two-particle operator $\hat{b}_2$ can be expressed as

$$\hat{B}_2 = \frac{1}{2!}\sum_{i,j,k,l=1}^{M} \underbrace{\langle i\,j|\,\hat{b}_2\,|k\,l\rangle}_{b_{ijkl}}\,\hat{c}_i^{\dagger}\,\hat{c}_j^{\dagger}\,\hat{c}_l\,\hat{c}_k\;, \tag{2.7}$$

and so forth for n-particle operators.
The Hamilton operator, consisting of the single-particle operators $\hat{T}$ and $\hat{V}$ and the two-particle operator $\hat{W}$ can thus be written as

$$\hat{H}(t) = \sum_{ij} h_{ij}^{(0)}\hat{c}_i^{\dagger}\hat{c}_j + \frac{1}{2}\sum_{ijkl} w_{ijkl}\hat{c}_i^{\dagger}\hat{c}_j^{\dagger}\hat{c}_l\hat{c}_k \tag{2.8}$$

where $\hat{H}^{(0)} = \hat{T} + \hat{V}$ and $h_{ij}^{(0)} = \langle i|\hat{H}^{(0)}|j\rangle$.
The dynamics of the system can then be described by considering the Heisenberg creation and annihilation operators

$$\hat{c}_{\mathrm{H}}^{(\dagger)}(t) = \hat{U}^{\dagger}(tt_0)\hat{c}^{(\dagger)}\hat{U}(tt_0)\;, \tag{2.9}$$

where

$$\hat{U}(t_1,t_2) = \mathcal{T}\exp\left(-\frac{\mathrm{i}}{\hbar}\int_{t_2}^{t_1}\mathrm{d}\bar{t}\,\hat{H}(\bar{t})\right) \tag{2.10}$$

is the time propagation operator and $\mathcal{T}$ is the time-ordering operator. Their equation of motion is given by the Heisenberg equation

$$\mathrm{i}\hbar\partial_t\hat{c}_{\mathrm{H}}^{(\dagger)}(t) = -\hat{U}^{\dagger}\left[\hat{H},\hat{c}^{(\dagger)}\right]\hat{U}(tt_0)\;. \tag{2.11}$$

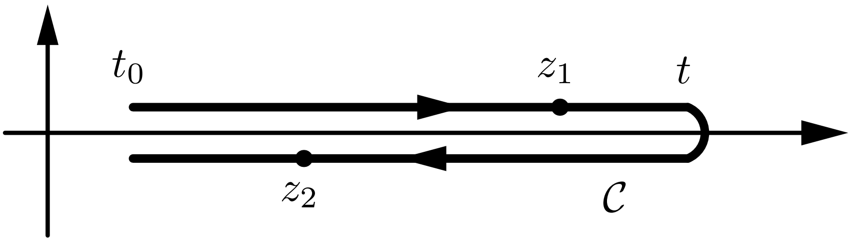

Figure 2.1: Illustration of the two real-time branches of the Keldysh contour. z_1 on the causal branch $\mathcal{C}_-$ is earlier on the contour than z_2 on the anticausal branch $\mathcal{C}_+$, although the physical time corresponding to z_1 is later than the physical time corresponding to z_2. (Figure taken from Ref. [17].)

Using the commutation relations (2.4) and (2.5), this becomes

$$\mathrm{i}\hbar\partial_t \hat{c}_{i\mathrm{H}}(t) = \sum_l h^{(0)}_{il}\hat{c}_{l\mathrm{H}}(t) + \underbrace{\sum_{lmn} w_{imln}\hat{c}^{\dagger}_{m\mathrm{H}}(t)\hat{c}_{n\mathrm{H}}(t)}_{v^{\mathrm{eff}}_{il}(t)}\,\hat{c}_{l\mathrm{H}}(t) \tag{2.12}$$

and its adjoint.

2.2 Nonequilibrium Green Functions

The Green functions formalism is used for the statistical treatment of quantum mechanical many-particle systems. The nonequilibrium Green function is defined as the ensemble average of a time-ordered product of creation and annihilation operators. Its dynamics is described by its equations of motion and it can be used to calculate most statistical properties of the system. This approach is not inherently less complex than other approaches, but it does make it possible to find approximations by reducing the formalism to the calculation of the one-particle Green function $\mathrm{G}^{(1)}$.

2.2.1 The Keldysh Contour $\mathcal{C}$

Let $\hat{A}_{\mathrm{H}}$ be a single-particle Heisenberg operator in second quantization:

$$\begin{aligned}\hat{A}_{\mathrm{H}} &= \hat{U}(t_0,t)\hat{A}_{\mathrm{S}}\hat{U}(t,t_0) = \sum_{ij} a_{ji}\hat{U}(t_0,t)\hat{c}^{\dagger}_j\hat{c}_i\hat{U}(t,t_0) \\ &= \sum_{ij} a_{ji}\hat{U}(t_0,t)\hat{c}^{\dagger}_j\hat{U}(t,t_0)\hat{U}(t_0,t)\hat{c}_i\hat{U}(t,t_0) = \sum_{ij} a_{ji}\hat{c}^{\dagger}_{j\mathrm{H}}\hat{c}_{i\mathrm{H}}\ ,\end{aligned} \tag{2.13}$$

The ensemble average of $\hat{A}_{\mathrm{H}}$ is given by

$$\left\langle \hat{A}_{\mathrm{H}} \right\rangle = \sum_{ji} a_{ji}\left\langle \hat{c}^{\dagger}_{j\mathrm{H}}\hat{c}_{i\mathrm{H}} \right\rangle\ . \tag{2.14}$$

The Heisenberg operators can be expressed in terms of their Schrödinger equivalents as

$$\begin{aligned}\hat{c}^{\dagger}_{j\mathrm{H}}(t)\hat{c}_{i\mathrm{H}}(t) &= \hat{U}(t_0,t)\hat{c}^{\dagger}_{j\mathrm{S}}\hat{c}_{i\mathrm{S}}\hat{U}(t,t_0) \\ &= \bar{\mathcal{T}}\left\{\exp\left(-\frac{\mathrm{i}}{\hbar}\int_{t}^{t_0}\mathrm{d}\bar{t}\,\hat{H}(\bar{t})\right)\right\}\hat{c}^{\dagger}_{j\mathrm{S}}\hat{c}_{i\mathrm{S}}\mathcal{T}\left\{\exp\left(-\frac{\mathrm{i}}{\hbar}\int_{t_0}^{t}\mathrm{d}\bar{t}\,\hat{H}(\bar{t})\right)\right\}\ , \end{aligned} \tag{2.15}$$

where $\mathcal{T}$ and $\bar{\mathcal{T}}$ are the causal and anti-causal time-ordering operators. It is possible to identify the time propagation operators in Eq. (2.15) with a single time propagation operator on a time contour called the Keldysh contour, consisting of a causal and an anticausal branch, as illustrated in Fig. 2.1, if the operators in Eq. (2.15) are time-ordered on the contour.

$$\left\langle \hat{c}^{\dagger}_{j\mathrm{H}}\hat{c}_{i\mathrm{H}}\right\rangle = \frac{1}{Z_0}\mathrm{Tr}\left\{\exp(\beta\mu\hat{N}_{\mathrm{S}})\mathcal{T}_{\mathcal{C}}\left[\exp\left(-\frac{\mathrm{i}}{\hbar}\int_{\mathcal{C}}\mathrm{d}\bar{z}\hat{H}_{\mathrm{S}}(\bar{z})\right)\hat{c}^{\dagger}_{j\mathrm{S}}(z)\hat{c}_{i\mathrm{S}}(z)\right]\right\}\ . \tag{2.16}$$

2.2.2 The n-Particle Correlator and its Equations of Motion

In second quantization, the matrix elements $\hat{G}^{(n)}_{i_1...i_nj_1...j_n}$ of the n-particle correlator $\hat{\mathrm{G}}^{(n)}$ can be written as

$$\hat{G}^{(n)}_{i_1...i_nj_1...j_n}(z_1...z_n;z'_1...z'_n) = \left(-\frac{\mathrm{i}}{\hbar}\right)^n\mathcal{T}_{\mathcal{C}}\left\{\hat{c}_{i_1}(z_1)...\hat{c}_{i_n}(z_n)\hat{c}^{\dagger}_{j_n}(z'_n)...\hat{c}^{\dagger}_{j_1}(z'_1)\right\}\ . \tag{2.17}$$

Its equations of motion can be derived from the equations of motion of the field operators $\hat{c}$ and $\hat{c}^{\dagger}$ (eq. (2.12)) and are given by

$$\begin{aligned}&\left[\mathrm{i}\hbar\partial_{z_k} - h^{(0)}(z_k)\right]\hat{\mathrm{G}}^{(n)}(z_1...z_n;z'_1...z'_n) = \\ &\pm\mathrm{i}\hbar\int_{\mathcal{C}}\mathrm{d}\bar{z}\,W(z_k\bar{z})\hat{\mathrm{G}}^{(n+1)}(z_1...z_n\bar{z};z'_1...z'_n\bar{z}^{+}) \\ &+\sum_{p=1}^{n}(\pm 1)^{k+p}\delta_{\mathcal{C}}(z_kz'_p)\hat{\mathrm{G}}^{(n-1)}(z_1...\cancel{z_k}...z_n;z'_1...\cancel{z'_p}...z'_n)\end{aligned} \tag{2.18}$$

and

$$\begin{aligned}&\hat{\mathrm{G}}^{(n)}(z_1...z_n;z'_1...z'_n)\left[-\mathrm{i}\hbar\overleftarrow{\partial}_{z'_k} - h^{(0)}(z'_k)\right] = \\ &\pm\mathrm{i}\hbar\int_{\mathcal{C}}\mathrm{d}\bar{z}\,\hat{\mathrm{G}}^{(n+1)}(z_1...z_n\bar{z}^{-};z'_1...z'_n\bar{z})W(\bar{z}z'_k) \\ &+\sum_{p=1}^{n}(\pm 1)^{k+p}\delta_{\mathcal{C}}(z_pz'_k)\hat{\mathrm{G}}^{(n-1)}(z_1...\cancel{z_p}...z_n;z'_1...\cancel{z'_k}...z'_n)\ ,\end{aligned} \tag{2.19}$$

where $W(z_1,z_2) = \delta_{\mathcal{C}}(z_1,z_2)w(z_1)$ and w is the interaction operator introduced in eq. (2.8). The arrow in $\overleftarrow{\partial}_{z'_k}$ means that the differential operator is acting to the left, i.e., on $\hat{\mathrm{G}}^{(n)}(z_1...z_n;z'_1...z'_n)$.
With $\hat{\mathrm{G}}^{(0)} = \mathbb{1}$, these equations are well defined.

2.2.3 Nonequilibrium Green Functions, the Martin–Schwinger Hierarchy and the Kadanoff–Baym Equations

The n-particle Green function is defined as the ensemble average of the n-particle correlator:

$$\mathrm{G}^{(n)} = \left\langle \hat{\mathrm{G}}^{(n)} \right\rangle \ , \tag{2.20}$$

therefore

$$G^{(n)}_{i_1..i_n;j_1..j_n}(z_1...z_n;z'_1...z'_n) = \left(-\frac{\mathrm{i}}{\hbar}\right)^n \left\langle \hat{\mathcal{T}}_{\mathcal{C}} \hat{c}_{i_1}(z_1)...\hat{c}_{i_n}(z_n)\hat{c}^\dagger_{j_n}(z'_n)...\hat{c}^\dagger_{j_1}(z'_1) \right\rangle \ . \tag{2.21}$$

Its equations of motion are formally identical to the equations of motion of the correlator

$$\begin{aligned}
&\left[\mathrm{i}\hbar\partial_{z_k} - h^{(0)}(z_k)\right] \mathrm{G}^{(n)}(z_1...z_n;z'_1...z'_n) = \\
&\pm \mathrm{i}\hbar \int_{\mathcal{C}} \mathrm{d}\bar{z}\, W(z_k\bar{z})\mathrm{G}^{(n+1)}(z_1...z_n\bar{z};z'_1...z'_n\bar{z}^+) \\
&+ \sum_{p=1}^{n} (\pm 1)^{k+p} \delta_{\mathcal{C}}(z_k z'_p) \mathrm{G}^{(n-1)}(z_1...\cancel{z_k}...z_n;z'_1...\cancel{z'_p}...z'_n)
\end{aligned} \tag{2.22}$$

and

$$\begin{aligned}
&\mathrm{G}^{(n)}(z_1...z_n;z'_1...z'_n) \left[-\mathrm{i}\hbar\overleftarrow{\partial}_{z'_k} - h^{(0)}(z'_k)\right] = \\
&\pm \mathrm{i}\hbar \int_{\mathcal{C}} \mathrm{d}\bar{z}\, \mathrm{G}^{(n+1)}(z_1...z_n\bar{z}^-;z'_1...z'_n\bar{z})W(\bar{z}z'_k) \\
&+ \sum_{p=1}^{n} (\pm 1)^{k+p} \delta_{\mathcal{C}}(z_p z'_k) \mathrm{G}^{(n-1)}(z_1...\cancel{z_p}...z_n;z'_1...\cancel{z'_k}...z'_n) \ .
\end{aligned} \tag{2.23}$$

This hierarchy of equations is called the Martin–Schwinger hierarchy.
These equations for $\mathrm{G}^{(1)}$ are not closed, since they depend on the two-particle Green function $\mathrm{G}^{(2)}$. The equations of motion for $\mathrm{G}^{(2)}$ depend on $\mathrm{G}^{(1)}$ and $\mathrm{G}^{(3)}$, and so forth; the equations for the n-particle Green function depend on the equations for the $(n-1)$- and the $(n+1)$-particle Green functions. The first two hierarchy equations can be formally closed by the introduction of the selfenergy Σ, which is taken to be a functional of the single particle Green function by the identification:

$$\pm \mathrm{i}\hbar \int_{\mathcal{C}} \mathrm{d}\bar{z}\, W(z\bar{z})\mathrm{G}^{(2)}(z\bar{z}z'\bar{z}^+) = \int_{\mathcal{C}} \mathrm{d}\bar{z}\, \Sigma(z\bar{z})\mathrm{G}^{(1)}(\bar{z}z') \tag{2.24}$$

$$\pm \mathrm{i}\hbar \int_{\mathcal{C}} \mathrm{d}\bar{z}\, \mathrm{G}^{(2)}(z\bar{z}^-z'\bar{z})W(\bar{z}z') = \int_{\mathcal{C}} \mathrm{d}\bar{z}\, \mathrm{G}^{(1)}(z\bar{z})\Sigma(\bar{z}z') \ . \tag{2.25}$$

The resulting equations are:

$$\left[\mathrm{i}\hbar\partial_z - h(z)\right] \mathrm{G}^{(1)}(zz') = \delta_{\mathcal{C}}(zz')\mathbb{1} + \int_{\mathcal{C}} \mathrm{d}\bar{z}\, \Sigma(z\bar{z})\mathrm{G}^{(1)}(\bar{z}z') \ , \tag{2.26}$$

and its adjoint,

$$\left[-\mathrm{i}\hbar\partial_{z'} - h(z)\right] \mathrm{G}^{(1)}(zz') = \delta_{\mathcal{C}}(zz')\mathbb{1} + \int_{\mathcal{C}} \mathrm{d}\bar{z}\, \mathrm{G}^{(1)}(z\bar{z})\Sigma(\bar{z}z') \ . \tag{2.27}$$

They are known as the Kadanoff–Baym equations.

2.2.4 Approximations to the Selfenergy Σ

There are several well known methods for approximating the selfenergy, only a few of which are treated explicitly in this thesis. These are, in increasing order of complexity, the Hartree–Fock selfenergy Σ^{HF}, the second Born selfenergy Σ^{SOA} and the T-matrix selfenergy Σ^{TPP}. 'SOA' stands for 'second order approximation', since the second Born approximation is exact in second order. The 'PP' in 'TPP' stands for 'particle-particle channel'. The approximation is named that way because only diagrams describing particle-particle (and hole-hole) interaction are taken into consideration, other interactions are neglected, such as particle-hole interactions.
Σ^{HF} is defined as

$$\Sigma^{\mathrm{HF}}(zz') = \pm \mathrm{i}\hbar\delta_{\mathcal{C}}(zz')\int_{\mathcal{C}} \mathrm{d}\bar{z}\, W(z\bar{z})\mathrm{G}^{(1)}(\bar{z}\bar{z}^{+}) + \mathrm{i}\hbar\mathrm{G}^{(1)}(zz')W(z^{+}z') \ . \tag{2.28}$$

The matrix multiplication are defined such that

$$\left[W\mathrm{G}^{(1)}\right]_{ij} = \sum_{k,l} w_{ikjl}G_{lk} \tag{2.29}$$

and

$$\left[\mathrm{G}^{(1)}W\right]_{ij} = \sum_{k,l} G_{lk}w_{iklj} \ . \tag{2.30}$$

The Hartree-Fock approximation stems from approximating the two-particle Green function as an (anti-)symmetrized product of single-particle Green functions in the following way:

$$G^{(2),\,\mathrm{HF}}_{ijkl}(z_1z_2, z_1'z_2') = G^{(1)}_{ik}(z_1z_1')G^{(1)}_{jl}(z_2z_2') \pm G^{(1)}_{il}(z_1z_2')G^{(1)}_{jk}(z_2z_1') \ . \tag{2.31}$$

The Hartree–Fock approximation describes mean-field and exchange processes and neglects all other correlation effects, which is only appropriate for small interaction strengths.
Amongst the more complex approximations that describe more correlation effects and that are applicable for greater interaction strengths, there are the second Born and T-matrix selfenergies. The second Born selfenergy Σ^{SOA} is defined as:

$$\begin{aligned}
&\Sigma^{\mathrm{SOA}}(zz') = \\
&(\mathrm{i}\hbar)^2\int_{\mathcal{C}}\int_{\mathcal{C}} \mathrm{d}\bar{z}\mathrm{d}\bar{\bar{z}}\, \mathrm{G}^{(1)}(z\bar{z})W(z^{+}\bar{\bar{z}})\mathrm{G}^{(1)}(\bar{z}\bar{\bar{z}})\mathrm{G}^{(1)}(\bar{\bar{z}}z')W(\bar{z}^{+}z') \\
&\pm(\mathrm{i}\hbar)^2\int_{\mathcal{C}}\int_{\mathcal{C}} \mathrm{d}\bar{z}\mathrm{d}\bar{\bar{z}}\, \mathrm{G}^{(1)}(zz')W(z^{+}\bar{z})W(z'\bar{\bar{z}})\mathrm{G}^{(1)}(\bar{\bar{z}}\bar{z})\mathrm{G}^{(1)}(\bar{z}\bar{\bar{z}}^{+}) \ .
\end{aligned} \tag{2.32}$$

The TPP selfenergy is defined as follows:

$$\Sigma^{\mathrm{TPP}} = \mathrm{i}\hbar T(zz')\mathrm{G}^{(1)}(z'z) \ , \tag{2.33}$$

where T is described by the following equation of motion (the Lippmann–Schwinger equation):

$$T(zz') = \pm\mathrm{i}\hbar W(z)\mathrm{G}^{\mathrm{H}}(zz')W^{\pm}(z) + \mathrm{i}\hbar\int_{\mathcal{C}}\mathrm{d}\bar{z}\, W(z)\mathrm{G}^{\mathrm{H}}(z\bar{z})T(\bar{z}z') \ , \tag{2.34}$$

$W^{\pm}_{ijkl}(z) = W_{ijkl}(z) \pm W_{ijlk}(z)$ and $G^{\mathrm{H}}_{ijkl}(zz') = G^{(1)}_{ik}(zz')G^{(1)}_{jl}(zz')$.

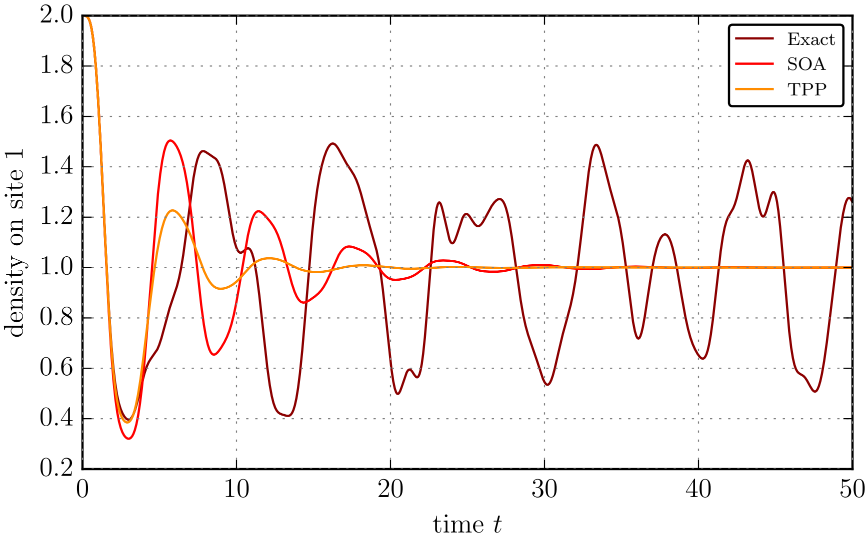

Figure 2.2: Correlation-induced damping in SOA and TPP simulations compared to the results of exact diagonalization. The figure shows the density evolution on the first of four sites in a one-dimensional Hubbard chain that initially contained one spin-up and one spin-down electron in each of the first two sites. The interaction strength $U = 1$.

2.2.5 The Generalized Kadanoff–Baym Ansatz

The approximations treated in the previous section, particularly the second Born (SOA) and T-matrix (TPP) selfenergies, are very useful for numerical applications. They do, however, have several disadvantages. First of all they are numerically expensive, the computing time of both SOA and TPP simulations scales cubically with the number of timesteps[17]. But there is also another problem: Some systems, in particular small, strongly interacting clusters, tend towards damped states that do not arise in the exact calculations[5]. This can be seen in Fig. 2.2, for example. One solution to both of these problems is to use a further approximation called the generalized Kadanoff–Baym ansatz (GKBA) that reduces the propagation to the time-diagonal part of the Green functions, becoming, in turn, much faster[13]. Figure 2.3 shows how the damping observed in Fig. 2.2 disappears in GKBA simulations.

To understand the GKBA in some more detail[1] it is necessary to introduce the real-time components of the (single-particle) Green function. There exist four different ways of ordering two real time arguments $t_1 < t_2$ on the Keldysh contour, i.e., assigning them different z_1, z_2 corresponding to the same physical times:

- z_1 and z_2 could both be on the causal branch $\mathcal{C}_-$, which leads to the causal component G^{c}

---

[1] This is still only a very brief introduction, for more detail and the full derivation, see for instance Ref. [13].

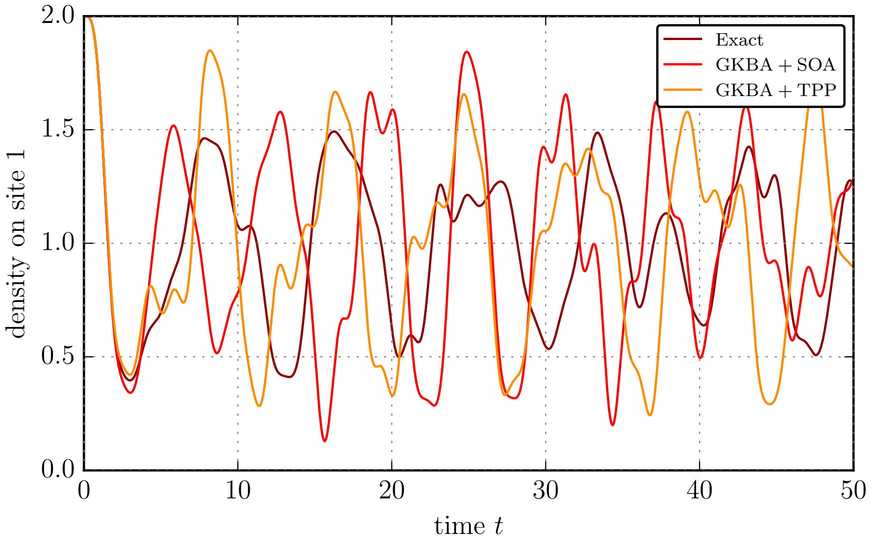

Figure 2.3: Correlation-induced damping in GKBA+SOA and GKBA+TPP simulations compared to the results of exact diagonalization. The figure shows the density evolution on the first of four sites in a one-dimensional Hubbard chain that initially contained one spin-up and one spin-down electron in each of the first two sites. The interaction strength $U = 1$.

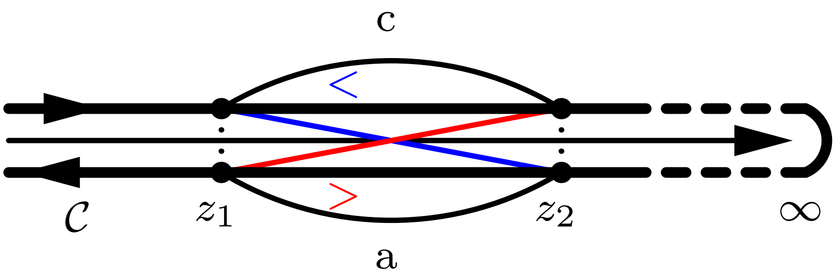

Figure 2.4: Illustration of the real-time components of the single-particle Green function. They stem from the fact that there are four different ways of ordering two real time arguments on the Keldysh contour. Figure taken from Ref. [17]

- z_1 and z_2 could both be on the anticausal branch $\mathcal{C}_+$, which leads to the anticausal component G^{a}
- z_1 could be on the causal branch and z_2 on the anticausal branch, which leads to the lesser component $\mathrm{G}^<$
- and vice versa, which leads to the greater component $\mathrm{G}^>$.

This is illustrated in Fig. 2.4. The components can be defined element-wise as

$$G^{\mathrm{c}}_{ij}(t_1t_2) = -\frac{\mathrm{i}}{\hbar}\left\langle \mathcal{T}\left[\hat{c}_i(t_1)\hat{c}^\dagger_j(t_2)\right]_-\right\rangle \,, \tag{2.35}$$

$$G^{\mathrm{a}}_{ij}(t_1t_2) = -\frac{\mathrm{i}}{\hbar}\left\langle \bar{\mathcal{T}}\left[\hat{c}_i(t_1)\hat{c}^\dagger_j(t_2)\right]_-\right\rangle \,, \tag{2.36}$$

$$G^{<}_{ij}(t_1t_2) = +\frac{\mathrm{i}}{\hbar}\left\langle \hat{c}^\dagger_j(t_2)\hat{c}_i(t_1)\right\rangle \,, \tag{2.37}$$

$$G^{>}_{ij}(t_1t_2) = +\frac{\mathrm{i}}{\hbar}\left\langle \hat{c}_i(t_1)\hat{c}^\dagger_j(t_2)\right\rangle \,. \tag{2.38}$$

It is useful, however, to define two further quantities, the retarded and advanced Green functions G^{R} and G^{A} and to use them instead of G^{a} and G^{c}. They are defined as

$$\mathrm{G}^{\mathrm{R}}(t_1t_2) = \mathrm{G}^{\mathrm{c}}(t_1t_2) - \mathrm{G}^<(t_1t_2) = \mathrm{G}^>(t_1t_2) - \mathrm{G}^{\mathrm{a}}(t_1t_2)\,, \tag{2.39}$$

$$\mathrm{G}^{\mathrm{A}}(t_1t_2) = \mathrm{G}^{\mathrm{c}}(t_1t_2) - \mathrm{G}^>(t_1t_2) = \mathrm{G}^<(t_1t_2) - \mathrm{G}^{\mathrm{a}}(t_1t_2)\,. \tag{2.40}$$

The equations of motion are then given by

$$\left[\mathrm{i}\hbar\partial_t - h^{(0)}(t)\right]\mathrm{G}^{\gtrless}(tt') = \int_{t_0}^{\infty}\mathrm{d}\bar{t}\,\left\{\Sigma^{\mathrm{R}}(t\bar{t})\mathrm{G}^{\gtrless}(\bar{t}t') + \Sigma^{\gtrless}(t\bar{t})\mathrm{G}^{\mathrm{A}}(\bar{t}t')\right\}\,, \tag{2.41}$$

$$\mathrm{G}^{\gtrless}(tt')\left[-\mathrm{i}\hbar\overleftarrow{\partial}_{t'} - h^{(0)}(t')\right] = \int_{t_0}^{\infty}\mathrm{d}\bar{t}\,\left\{\mathrm{G}^{\mathrm{R}}(t\bar{t})\Sigma^{\gtrless}(\bar{t}t') + \mathrm{G}^{\gtrless}(t\bar{t})\Sigma^{\mathrm{A}}(\bar{t}t')\right\}\,, \tag{2.42}$$

$$\left[\mathrm{i}\hbar\partial_t - h^{(0)}(t)\right]\mathrm{G}^{\mathrm{R/A}}(tt') = \delta(tt') + \int_{t_0}^{\infty}\mathrm{d}\bar{t}\,\Sigma^{\mathrm{R/A}}(t\bar{t})\,\mathrm{G}^{\mathrm{R/A}}(\bar{t}t')\,, \tag{2.43}$$

$$\mathrm{G}^{\mathrm{R/A}}(tt')\left[-\mathrm{i}\hbar\overleftarrow{\partial}_{t'} - h^{(0)}(t')\right] = \delta(tt') + \int_{t_0}^{\infty}\mathrm{d}\bar{t}\,\mathrm{G}^{\mathrm{R/A}}(t\bar{t})\Sigma^{\mathrm{R/A}}(\bar{t}t')\,. \tag{2.44}$$

From these equations can be derived that

$$\begin{aligned}\mathrm{G}^{\gtrless}(t_1t_2) = {} & \pm\left[\mathrm{G}^{\mathrm{R}}(t_1t_2)n^{\gtrless}(t_2) - n^{\gtrless}(t_1)\mathrm{G}^{\mathrm{A}}(t_1t_2)\right] \\ & + \int_{t_2}^{t_1}\mathrm{d}\bar{t}_1\int_{t_0}^{t_2}\mathrm{d}\bar{t}_2\,\mathrm{G}^{\mathrm{R}}(t_1\bar{t}_1)\Sigma^{\mathrm{R}}(\bar{t}_1\bar{t}_2)\mathrm{G}^{\gtrless}(\bar{t}_2t_2) \\ & + \int_{t_2}^{t_1}\mathrm{d}\bar{t}_1\int_{t_0}^{t_2}\mathrm{d}\bar{t}_2\,\mathrm{G}^{\mathrm{R}}(t_1\bar{t}_1)\Sigma^{\gtrless}(\bar{t}_1\bar{t}_2)\mathrm{G}^{\mathrm{A}}(\bar{t}_2t_2) \\ & + \int_{t_2}^{t_1}\mathrm{d}\bar{t}_1\int_{t_0}^{t_2}\mathrm{d}\bar{t}_2\,\mathrm{G}^{\gtrless}(t_1\bar{t}_1)\Sigma^{\mathrm{A}}(\bar{t}_1\bar{t}_2)\mathrm{G}^{\mathrm{A}}(\bar{t}_2t_2) \\ & + \int_{t_2}^{t_1}\mathrm{d}\bar{t}_1\int_{t_0}^{t_2}\mathrm{d}\bar{t}_2\,\mathrm{G}^{\mathrm{R}}(t_1\bar{t}_1)\Sigma^{\gtrless}(\bar{t}_1\bar{t}_2)\mathrm{G}^{\mathrm{A}}(\bar{t}_2t_2)\,,\end{aligned} \tag{2.45}$$

where

$$n^{>} = n - \mathbb{1}, \quad n^{<} = n \; , \tag{2.46}$$

and where n is the density and

$$n^{\gtrless}(t) = -\mathrm{i}\hbar \mathrm{G}^{\gtrless}(tt) \; . \tag{2.47}$$

The generalized Kadanoff–Baym ansatz consists of neglecting the integral terms in Eq. (2.45)[18], yielding

$$\mathrm{G}^{\gtrless}(t_1 t_2) \approx \pm \left[\mathrm{G}^{\mathrm{R}}(t_1 t_2) n^{\gtrless}(t_2) - n^{\gtrless}(t_1) \mathrm{G}^{\mathrm{A}}(t_1 t_2) \right] \; , \tag{2.48}$$

and finding suitable approximations for the propagators G^{R} and G^{A}.

2.2.6 The Calculation of some Statistical Properties from the Green Functions

In later sections, some statistical properties are analysed. It is therefore important to know how they are derived from the (single-particle) Green function. The quantities in question are the density n, the kinetic energy E_{kin}, the Hartree–Fock energy E_{HF}, the correlation energy E_{corr} and the entanglement entropy S. It is

$$n_{ij} = \pm \mathrm{i} G^{<}_{ij}(tt^{+}) \tag{2.49}$$

$$E_{\mathrm{kin}}(t) = \mathrm{Re}\left[\mathrm{Tr}\left(h^{(0)} n(t) \right) \right] \; , \tag{2.50}$$

$$E_{\mathrm{HF}}(t) = \frac{1}{2} \mathrm{Re}\left[\mathrm{Tr}\left(\Sigma^{\mathrm{HF}}(t) n(t) \right) \right] \; , \tag{2.51}$$

$$E_{\mathrm{corr}}(t) = \frac{1}{2} \mathrm{Im}\left[\mathrm{Tr}\left(I^{(1),<}(t,t) \right) \right] \; , \tag{2.52}$$

where $I^{(1),<}(t,t)$ is the time-diagonal collision integral

$$I^{(1),<}(t,t) = \int_{t_0}^{\infty} \mathrm{d}\bar{t} \left\{ \Sigma^{\mathrm{R}}(t\bar{t}) \mathrm{G}^{<}(\bar{t}t) + \Sigma^{<}(t\bar{t}) \mathrm{G}^{\mathrm{A}}(\bar{t}t) \right\} \; . \tag{2.53}$$

Furthermore, it is

$$\begin{aligned} S(t) = \sum_i -2 \left(\frac{1}{2} n_i(t) - n^{(2)}_{ii}(t) \right) \log_2 \left(\frac{n_i(t)}{2} - n^{(2)}_{ii}(t) \right) \\ - n^{(2)}_{ii}(t) \log_2 n^{(2)}_{ii}(t) - \left(1 - n_i(t) + n^{(2)}_{ii}(t) \right) \log_2 \left(1 - n_i(t) + n^{(2)}_{ii}(t) \right) \; , \end{aligned} \tag{2.54}$$

where

$$n^{(2)}_{ii} = \frac{1}{2U(t)} \left(\mathrm{Re}\left[\Sigma^{\mathrm{HF}}_i(t) n_i(t) \right] + \mathrm{Im}\left[I^{(1),<}_{ii}(t,t) \right] \right)$$

is the double occupation of site i.
Both the correlation energy and the entanglement entropy are measures of the correlation of the system.

2.3 Time Reversal Invariance

2.3.1 Time Reversal Invariance of Classical Systems

Time-reversal invariance in classical Hamiltonian systems is defined as follows[19]: If $(\mathbf{q}(t), \mathbf{p}(t))$ is a solution to the Hamilton equations

$$\begin{aligned} \dot{q}_i &= +\frac{\partial H}{\partial p_i} \ , \\ \dot{p}_i &= -\frac{\partial H}{\partial q_i} \ , \end{aligned}$$

then there exists another solution $(\mathbf{q}'(t'), \mathbf{p}'(t'))$ with $t' = -t$ and $\mathbf{q}' = \mathbf{q}'(\mathbf{q}), \mathbf{p}' = \mathbf{p}'(\mathbf{p})$. This defines a whole range of invariances depending on the nature of the relation between $\mathbf{q}$ and $\mathbf{q}'$, and that between $\mathbf{p}$ and $\mathbf{p}'$. The most intuitive and best-known of these invariances is the one that maps

$$\begin{aligned} \mathbf{q} \rightarrow \mathbf{q}' &= \mathbf{q} \ , \\ \mathbf{p} \rightarrow \mathbf{p}' &= -\mathbf{p} \ . \end{aligned}$$

This particular symmetry (referred to as conventional time reversal) is broken in the presence of a magnetic field, for instance. This does not, however, mean that such a system is not time reversal invariant, although not every Hamiltonian system is.
For quantum mechanical systems, similar things hold true, as shall be seen in the next section.

2.3.2 Time Reversal Invariance of Quantum Systems

The Schrödinger equation is called symmetric with regard to time reversal if for any solution $|\psi(t)\rangle$ there is another solution $|\psi'(t')\rangle$ with $t' = -t$ and if there is a unique relation between $|\psi\rangle$ and $|\psi'\rangle$ such that $|\psi'\rangle = \hat{T}|\psi\rangle$ for some operator $\hat{T}$[19]. It can be shown that $\hat{T}$ must not only be a linear operator, but an antiunitary one. Thus, it can be expressed as the product of complex conjugation and some unitary operator $\hat{U}$. The quantum mechanical equivalent to classical conventional time reversal is given by $\hat{U} = \mathbb{1}$, so that $|\psi\rangle \rightarrow |\psi\rangle^*$.
The time-dependent Schrödinger equation reads:

$$\mathrm{i}\hbar\partial_t|\psi\rangle = \hat{H}|\psi\rangle \ . \tag{2.55}$$

Applying $\hat{T}$ from both sides yiels:

$$\begin{aligned} \hat{T}\mathrm{i}\hbar\partial_t|\psi\rangle &= \hat{T}\hat{H}|\psi\rangle \\ \Leftrightarrow \underbrace{-\mathrm{i}\hbar\partial_t}_{\mathrm{i}\hbar\partial_{(-t)}}\hat{T}|\psi\rangle &= \hat{T}\hat{H}\hat{T}^{-1}\hat{T}|\psi\rangle \ , \end{aligned} \tag{2.56}$$

which means that $\hat{T}|\psi\rangle$ solves the time reversed Schrödinger equation

$$\mathrm{i}\hbar\partial_{(-t)}|\psi'\rangle = \hat{H}|\psi'\rangle \tag{2.57}$$

if (and only if) $\hat{H} = \hat{T}\hat{H}\hat{T}^{-1}$.

2.3.3 Time Reversal Invariance of the Heisenberg Equation

The Heisenberg equation is equivalent to the Schrödinger equation. It is therefore straightforward that it should have the same reversibilty properties:

$$\mathrm{i}\hbar\partial_t \hat{A}_{\mathrm{H}} = \left[\hat{A}_{\mathrm{H}}, \hat{H}\right] \tag{2.58}$$

$$\Leftrightarrow \hat{T}\mathrm{i}\hbar\partial_t \hat{A}_{\mathrm{H}}\hat{T}^{-1} = \hat{T}\left(\hat{A}_{\mathrm{H}}\hat{H} - \hat{H}\hat{A}_{\mathrm{H}}\right)\hat{T}^{-1}$$

$$\Leftrightarrow -\mathrm{i}\hbar\partial_t \hat{T}\hat{A}_{\mathrm{H}}\hat{T}^{-1} = \hat{T}\hat{A}_{\mathrm{H}}\hat{T}^{-1}\hat{T}\hat{H}\hat{T}^{-1} - \hat{T}\hat{H}\hat{T}^{-1}\hat{T}\hat{A}_{\mathrm{H}}\hat{T}^{-1}\ , \tag{2.59}$$

which is equivalent to

$$\mathrm{i}\hbar\partial_{-t}\hat{T}\hat{A}_{\mathrm{H}}\hat{T}^{-1} = \left[\hat{T}\hat{A}_{\mathrm{H}}\hat{T}^{-1}, \hat{H}\right] \tag{2.60}$$

if and only if $\hat{H} = \hat{T}\hat{H}\hat{T}^{-1}$. This means that if a Heisenberg operator $\hat{A}_{\mathrm{H}}(t)$ solves the Heisenberg equation, then $\hat{T}\hat{A}_{\mathrm{H}}\hat{T}^{-1}$ solves the time-reversed Heisenberg equation.

2.3.4 Time Reversal Invariance of the Equations of Motion of Field Operators in Second Quantization

The equation of motion of the annihilation operator in an arbitrary basis reads[15]:

$$\mathrm{i}\hbar\partial_t \hat{c}_i(t) = \sum_k \left[t_{ik} + v_{ik}(t)\right]\hat{c}_k(t) + \sum_{jkl} w_{ijkl}\hat{c}_j^\dagger(t)\hat{c}_l(t)\hat{c}_k(t)\ . \tag{2.61}$$

For the purpose of analysing time reversal symmetry, it is convenient to consider that Eq. (2.61) is derived from and equivalent to the Heisenberg equation for $\hat{c}(t)$:

$$\mathrm{i}\hbar\partial_t \hat{c}_i(t) = \left[\hat{c}_i, \hat{H}\right] \tag{2.62}$$

and, as such, possesses the same symmetry properties that $\hat{H}$ does. The same obviously holds for the creation operator $\hat{c}_j^\dagger$.
Furthermore, it can be shown that reversing time can be expressed by reversing the sign of the effective Hamiltonian in Eq. (2.61) by applying $\hat{T}$ from the left and $\hat{T}^{-1}$ from the right on both sides of the equation:

$$\begin{aligned} -\mathrm{i}\hbar\partial_t \left[\hat{T}\hat{c}\hat{T}^{-1}\right]_i &= \sum_k (t_{ik} + v_{ik})\left[\hat{T}\hat{c}\hat{T}^{-1}\right]_k \\ &+ \sum_{jkl} w_{ijkl}\left[\hat{T}\hat{c}^\dagger\hat{T}^{-1}\right]_j\left[\hat{T}\hat{c}\hat{T}^{-1}\right]_l\left[\hat{T}\hat{c}\hat{T}^{-1}\right]_k\ , \end{aligned}$$

assuming that not only $\hat{H} = \hat{T}\hat{H}\hat{T}^{-1}$ but that also $\hat{t} + \hat{v} = \hat{T}(\hat{t} + \hat{v})\hat{T}^{-1}$ and $\hat{w} = \hat{T}\hat{w}\hat{T}^{-1}$.

2.3.5 Time Reversal Invariance of the Martin–Schwinger Hierarchy

The analysis of time reversal symmetry in the Green functions formalism turns out to be rather more difficult than the previous considerations. There are, again, two questions of interest. First, whether reversing time in the equations is equivalent to reversing the Hamiltonian. Second, whether there exists a solution to the reversed equation and how it is related to the nonreversed solution.

Equivalence of reversing time and reversing the sign of the Hamiltonian

One of the first things to consider is how the δ-distribution transforms under time reversal. Since the δ-distribution is even with respect to its argument, i.e., $\delta(t) = \delta(-t)$, one could presume that it does not change at all. This cannot be true, as the following consideration shows:

$$\begin{aligned} \int_{\mathcal{C}} \mathrm{d}z\, \delta(z) = 1 \xrightarrow{z \to -z} 1 &= \int_{\mathcal{C}} \mathrm{d}(-z)\, \tilde{\delta}(z) \;, \\ \delta \xrightarrow{z \to -z} \tilde{\delta} &= -\delta \;. \end{aligned} \tag{2.63}$$

This means that the δ-distribution with respect to contour time arguments changes its sign under time reversal, similar to differential and integral operators. Considering now the first hierarchy equation and substituting $z \to -z$, $z' \to -z'$ yields:

$$\Big[-\mathrm{i}\hbar\partial_z - h(z) \Big] \mathrm{G}^{(1)}(z, z') \quad = -\delta_{\mathcal{C}}(z' - z)\mathbb{1} \pm \mathrm{i}\hbar \int_{\mathcal{C}} \mathrm{d}\bar{z}\, w(z^+, \bar{z}) \mathrm{G}^{(2)}(z\bar{z}, z'\bar{z}^+) \;, \tag{2.64}$$

since $w(z^+, \bar{z}) = \delta_{\mathcal{C}}(z^+, \bar{z}) w(z^+)$. This is equivalent to changing the sign of the Hamiltonian: $z(z') \to -z(-z') \Leftrightarrow \hat{H} \to -\hat{H}$. The same holds true for the second equation, as well as the higher-order hierarchy equations.

Existence of a solution to the reversed equation

The question remains whether these reversed equations have a solution and what, if any, the relation between this solution and the solution of the original, non-reversed equations is. It turns out to be easier to start by considering the n-particle correlators and their hierarchy of equations. Applying $\hat{T}$ from the left and $\hat{T}^{-1}$ from the right side of both sides of Eq. (2.22), as before, yields:

$$\begin{aligned} &\Big[-\mathrm{i}\hbar\partial_{z_k} - h^{(0)}(z_k) \Big] \hat{T}\hat{\mathrm{G}}^{(n)}\hat{T}^{-1}(z_1 ... z_n; z'_1 ... z'_n) = \\ &\mp \mathrm{i}\hbar \int_{\mathcal{C}} \mathrm{d}\bar{z}\, W(z_k\bar{z}) \hat{T}\hat{\mathrm{G}}^{(n+1)}\hat{T}^{-1}(z_1 ... z_n\bar{z}; z'_1 ... z'_n\bar{z}^+) \\ &+ \sum_{p=1}^{n} (\pm 1)^{k+p} \delta_{\mathcal{C}}(z_k z'_p) \hat{T}\hat{\mathrm{G}}^{(n-1)}\hat{T}^{-1}(z_1 ... \cancel{z_k} ... z_n; z'_1 ... \cancel{z'_p} ... z'_n) \;, \end{aligned} \tag{2.65}$$

where $\hat{T}\mathrm{G}^{\widehat{(n)}}\hat{T}^{-1}(z_1 ... z_n; z'_1 ... z'_n) = \hat{T} \left(\mathrm{G}^{\widehat{(n)}}(z_1 ... z_n; z'_1 ... z'_n) \right) \hat{T}^{-1}$. This is not equivalent to substituting $z^{(\prime)} \to -z^{(\prime)}$, therefore $\hat{T}\hat{\mathrm{G}}^{(n)}\hat{T}^{-1}$ does not solve the reversed equation. However, $\hat{\mathrm{G}}^{(n)}$ can be interpreted as a functional of creation and annihilation operators, $\hat{\mathrm{G}}^{(n)} = \hat{\mathrm{G}}^{(n)}\left[\hat{T}\hat{c}\hat{T}^{-1}, \hat{T}\hat{c}^{\dagger}\hat{T}^{-1}\right]$, and it is

$$\left[\hat{T}\hat{\mathrm{G}}^{(n)}\hat{T}^{-1}\right]_{i_1 \dots i_n j_1 \dots j_n}(z_1 \dots z_n; z'_1 \dots z'_n) = (-1)^n \left(-\frac{\mathrm{i}}{\hbar}\right)^n$$
$$\hat{\mathcal{T}}_{\mathcal{C}}\left\{\left[\hat{T}\hat{c}\hat{T}^{-1}\right]_{i_1}(z_1) \dots \left[\hat{T}\hat{c}\hat{T}^{-1}\right]_{i_n}(z_n)\left[\hat{T}\hat{c}^{\dagger}\hat{T}^{-1}\right]_{j_n}(z'_n) \dots \left[\hat{T}\hat{c}^{\dagger}\hat{T}^{-1}\right]_{j_1}(z'_1)\right\} . \tag{2.66}$$

Therefore

$$\hat{T}\hat{\mathrm{G}}^{(n)}\left[\hat{c}, \hat{c}^{\dagger}\right]\hat{T}^{-1} = (-1)^n \hat{\mathrm{G}}^{(n)}\left[\hat{T}\hat{c}\hat{T}^{-1}, \hat{T}\hat{c}^{\dagger}\hat{T}^{-1}\right] , \tag{2.67}$$

which means that $\hat{\mathrm{G}}^{(n)}\left[\hat{T}\hat{c}\hat{T}^{-1}, \hat{T}\hat{c}^{\dagger}\hat{T}^{-1}\right]$ does satisfy the reversed equation, because inserting this into Eq. (2.65) yields:

$$(-1)^n\left[-\mathrm{i}\hbar\partial_{z_k} - h^{(0)}(z_k)\right]\hat{\mathrm{G}}^{(n)}\left[\hat{T}\hat{c}\hat{T}^{-1}, \hat{T}\hat{c}^{\dagger}\hat{T}^{-1}\right](z_1 \dots z_n; z'_1 \dots z'_n) =$$
$$\mp (-1)^{n+1}\mathrm{i}\hbar\int_{\mathcal{C}} \mathrm{d}\bar{z}\, W(z_k\bar{z})\hat{\mathrm{G}}^{(n+1)}\left[\hat{T}\hat{c}\hat{T}^{-1}, \hat{T}\hat{c}^{\dagger}\hat{T}^{-1}\right](z_1 \dots z_n\bar{z}; z'_1 \dots z'_n\bar{z}^+)$$
$$+ (-1)^{n-1}\sum_{p=1}^{n}(\pm 1)^{k+p}\delta_{\mathcal{C}}(z_k z'_p)\hat{\mathrm{G}}^{(n-1)}\left[\hat{T}\hat{c}\hat{T}^{-1}, \hat{T}\hat{c}^{\dagger}\hat{T}^{-1}\right](z_1 \dots \cancel{z_k} \dots z_n; z'_1 \dots \cancel{z'_p} \dots z'_n) . \tag{2.68}$$

Dividing both sides of this equation by −1 yields the reversed equation (2.65). The same holds true for the adjoint equation (2.23). This is consistent with the way that creation and annihilation operators, which are Heisenberg operators, transform under time reversal, as seen in section 2.3.3.

From this follows directly, by taking the ensemble average of both sides, that $\mathrm{G}^{(n)}\left[\hat{T}\hat{c}\hat{T}^{-1}, \hat{T}\hat{c}^{\dagger}\hat{T}^{-1}\right]$ satisfies the reversed n^{th}-order equations of the Martin–Schwinger hierarchy in the same way.

2.3.6 Time Reversal Invariance of the Selfenergy

More precisely, this section treats the time reversal invariance of different approximations to the Kadanoff–Baym equations by different approximations to the selfenergy.

General Criterion

Substituting $z \to -z$, $z' \to -z'$ in the first Kadanoff–Baym equation (2.26) yields:

$$[-\mathrm{i}\hbar\partial_z - h(z)]\,\mathrm{G}^{(1)}(zz') = -\delta_{\mathcal{C}}(zz')\mathbb{1} - \int_{\mathcal{C}} \mathrm{d}\bar{z}\, \underbrace{\Sigma_{z^{(\prime)} \to -z^{(\prime)}}}_{\tilde{\Sigma}}(z\bar{z})\mathrm{G}^{(1)}(\bar{z}z') . \tag{2.69}$$

Substituting $\hat{H} \to -\hat{H}$ yields:

$$[\mathrm{i}\hbar\partial_z + h(z)]\,\mathrm{G}^{(1)}(zz') = \delta_{\mathcal{C}}(zz')\mathbb{1} + \int_{\mathcal{C}} \mathrm{d}\bar{z}\, \Sigma_{\hat{H} \to -\hat{H}}(z\bar{z})\mathrm{G}^{(1)}(\bar{z}z') , \tag{2.70}$$

which is equivalent to Eq. (2.69) if

$$\Sigma_{z^{(\prime)}\to -z^{(\prime)}} = \Sigma_{\hat{H}\to -\hat{H}} \; . \tag{2.71}$$

The Hartree–Fock Selfenergy

For the Hartree–Fock selfenergy Σ^{HF}, substituting $z \to -z$, $z' \to -z'$ yields:

$$\begin{aligned} \Sigma^{\mathrm{HF}}_{z^{(\prime)}\to -z^{(\prime)}}(zz') &= +\mathrm{i}\hbar\delta_{\mathcal{C}}(zz')\int_{\mathcal{C}} \mathrm{d}(-\bar{z})\,(-W(z\bar{z}))\mathrm{G}^{(1)}(\bar{z}\bar{z}^{+}) - \mathrm{i}\hbar W(z^{+}z')\mathrm{G}^{(1)}(zz') \\ &= \mathrm{i}\hbar\delta_{\mathcal{C}}(zz')\int_{\mathcal{C}} \mathrm{d}\bar{z}\, W(z\bar{z})\mathrm{G}^{(1)}(\bar{z}\bar{z}^{+}) - \mathrm{i}\hbar W(z^{+}z')\mathrm{G}^{(1)}(zz') \; . \end{aligned} \tag{2.72}$$

Substituting $\hat{H} \to -\hat{H}$ (and thereby substituting $W \to -W$) yields:

$$\begin{aligned} \Sigma^{\mathrm{HF}}_{\hat{H}\to -\hat{H}}(zz') &= -\mathrm{i}\hbar\delta_{\mathcal{C}}(zz')\int_{\mathcal{C}} \mathrm{d}\bar{z}\,(-W(z\bar{z}))\mathrm{G}^{(1)}(\bar{z}\bar{z}^{+}) + \mathrm{i}\hbar(-W(z^{+}z'))\mathrm{G}^{(1)}(zz') \\ &= \tilde{\Sigma}^{\mathrm{HF}}(zz') \; . \end{aligned} \tag{2.73}$$

The Second Born Selfenergy

For the second Born selfenergy Σ^{SOA}, substituting $z \to -z$, $z' \to -z'$ yields:

$$\begin{aligned} &\Sigma^{\mathrm{SOA}}_{z^{(\prime)}\to -z^{(\prime)}}(zz') \\ &= (\mathrm{i}\hbar)^2 \int_{\mathcal{C}}\int_{\mathcal{C}} d(-\bar{z})d(-\bar{\bar{z}})\,\mathrm{G}^{(1)}(z\bar{z})(-W(z^{+}\bar{\bar{z}}))\mathrm{G}^{(1)}(\bar{z}\bar{\bar{z}})\mathrm{G}^{(1)}(\bar{\bar{z}}z')(-W(\bar{z}^{+}z')) \\ &\quad - (\mathrm{i}\hbar)^2 \int_{\mathcal{C}}\int_{\mathcal{C}} d(-\bar{z})d(-\bar{\bar{z}})\,\mathrm{G}^{(1)}(zz')(-W(z^{+}\bar{z}))(-W(z'\bar{\bar{z}}))\mathrm{G}^{(1)}(\bar{\bar{z}}\bar{z})\mathrm{G}^{(1)}(\bar{z}\bar{\bar{z}}^{+}) \\ &= (\mathrm{i}\hbar)^2 \int_{\mathcal{C}}\int_{\mathcal{C}} d\bar{z}d\bar{\bar{z}}\,\mathrm{G}^{(1)}(z\bar{z})(-W(z^{+}\bar{\bar{z}}))\mathrm{G}^{(1)}(\bar{z}\bar{\bar{z}})\mathrm{G}^{(1)}(\bar{\bar{z}}z')(-W(\bar{z}^{+}z')) \\ &\quad - (\mathrm{i}\hbar)^2 \int_{\mathcal{C}}\int_{\mathcal{C}} d\bar{z}d\bar{\bar{z}}\,\mathrm{G}^{(1)}(zz')(-W(z^{+}\bar{z}))(-W(z'\bar{\bar{z}}))\mathrm{G}^{(1)}(\bar{\bar{z}}\bar{z})\mathrm{G}^{(1)}(\bar{z}\bar{\bar{z}}^{+}) \\ &= \Sigma^{\mathrm{SOA}}_{\hat{H}\to -\hat{H}}(zz') \; . \end{aligned} \tag{2.74}$$

The T-Matrix Selfenergy

For the T-matrix selfenergy to satisfy Eq. (2.71) the following must hold true:

$$T_{z^{(\prime)}\to -z^{(\prime)}} = T_{\hat{H}\to -\hat{H}} \; . \tag{2.75}$$

T is given by the Lippmann-Schwinger equation, which can be solved iteratively:

$$T^{0}(zz') = 0 \tag{2.76}$$

$$T^{n}(zz') = \pm\mathrm{i}\hbar W(z)G^{H}(zz')W^{\pm}(z) + \mathrm{i}\hbar\int_{\mathcal{C}} \mathrm{d}\bar{z}\, W(z)G^{H}(z\bar{z})T_{n-1}(\bar{z}z') \; . \tag{2.77}$$

The equivalence (2.75) can easily be shown by mathematical induction. The base case is trivial:

$$T^{0}_{z^{(\prime)}\to -z^{(\prime)}} = 0 = T^{0}_{\hat{H}\to -\hat{H}} \; . \tag{2.78}$$

Assuming $T^{n-1}_{z^{(\prime)}\to -z^{(\prime)}} = T^{n-1}_{\hat{H}\to-\hat{H}}$:

$$T^{n}_{z^{(\prime)}\to -z^{(\prime)}} = \pm \mathrm{i}\hbar W(z) G^{H}(zz') W^{\pm}(z) - \mathrm{i}\hbar \int_{\mathcal{C}} \mathrm{d}\bar{z}\, W(z) G^{H}(z\bar{z}) T^{z^{(\prime)}\to -z^{(\prime)}}_{n-1} \tag{2.79}$$

$$T^{n}_{\hat{H}\to-\hat{H}} = \pm \mathrm{i}\hbar W(z) G^{H}(zz') W^{\pm}(z) - \mathrm{i}\hbar \int_{\mathcal{C}} \mathrm{d}\bar{z}\, W(z) G^{H}(z\bar{z}) T^{\hat{H}\to-\hat{H}}_{n-1} \tag{2.80}$$

$$\Rightarrow T^{n}_{z^{(\prime)}\to -z^{(\prime)}} = T^{n}_{\hat{H}\to-\hat{H}}\ . \tag{2.81}$$

Thereby, not only do the full T-matrix and T-matrix selfenergy display the correct time reversal behaviour, but even when the series is truncated and $T \approx T^{N}$ for some $N \in \mathbb{N}$, as is done in numerical calculations, Eq. (2.71) is exactly satisfied.

3 Model System

3.1 The Hubbard Model

The Hubbard model is a greatly simplified approximation of condensed matter systems. In its limits, however, it is as powerful as it is instructive. In the model, solid state crystals are considered to be lattices of stationary atomic cores with overlapping outermost electronic orbitals[16]. Electrons in those outermost orbitals are able to tunnel from one site to the next with a probabilty proportional to the hopping parameter J. The assumpations of the Hubbard model are illustrated in Fig. 3.1 Interactions are assumed to be on-site only (an assumption which is justified by the lower orbital electrons shielding the potentials of the outer electrons). Tunnelling between non-neighbouring sites is neglected. The system can then be described in terms of occupation numbers of spin up and spin down electrons on each site, which yields a description in second quantization.

The Hubbard Hamiltonian takes the following form:

$$\hat{H}(t) = -J \sum_{\langle i,j \rangle} \sum_{\alpha} \hat{c}^{\dagger}_{i,\alpha} \hat{c}_{j,\alpha} + U \sum_{i} \hat{n}^{\uparrow}_{i} \hat{n}^{\downarrow}_{i} \ . \tag{3.1}$$

$\langle i, j \rangle$ denote neighbouring sites. The first term on the right hand side describes tunnelling processes as hopping from one site to another with an amplitude J. The second term describes on-site interaction of electrons with a given interaction strength U [17].

3.2 The Model System

The systems that have been simulated in this thesis are one-dimensional, four-site Hubbard chains, as illustrated in Fig. 3.2. Initially, one spin-up electron and one spin-down electron are deployed on each of the first two sites. The Hubbard hopping parameter $J = 1$. The Kadanoff–Baym equations (2.26) and (2.27) have been discretized and solved numerically in discrete time steps on the two-dimensional time plane in accordance with Fig. 3.3. For the selfenergy, the T-matrix approximation (2.33) has been chosen as an example. The initial state has been chosen to be an ideal, uncorrelated state.

For more details on the numerical implementation, see e.g. Ref. [17].

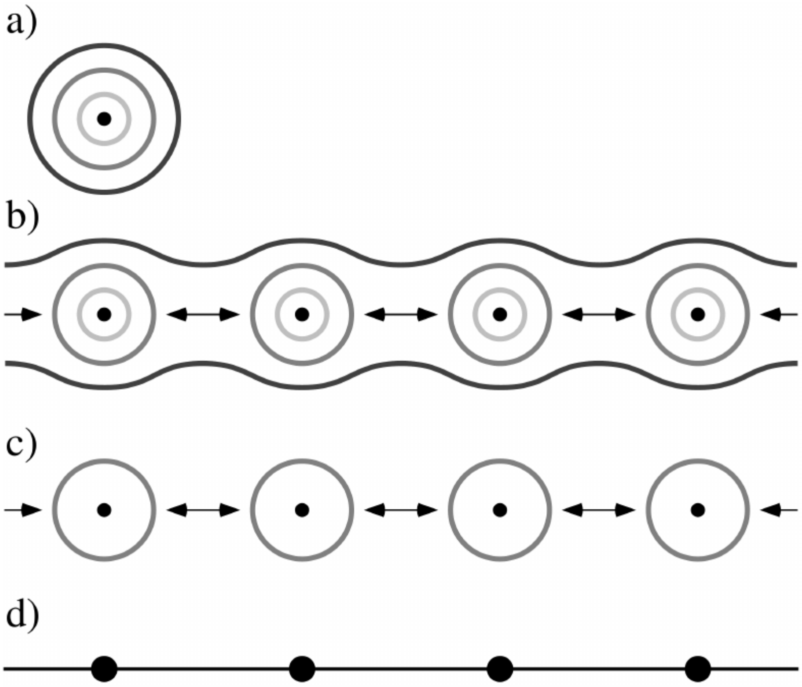

Figure 3.1: Illustration of the Hubbard model. In a), a single atom with nondegenerate electronic orbitals is shown. In b) a one-dimensional lattice of the same atom is shown, with the outermost orbitals overlapping. The arrows designate the capacity of the electrons in those orbitals to move between the atoms. In c), the inner orbitals cease to be considered except for their screening effects. d) shows the final model, as described in section 3.1. The figure is taken from Ref. [16].

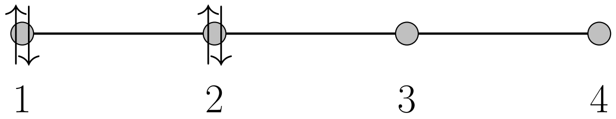

Figure 3.2: Illustration of the initial state of the system. The system consists of four atoms in a one-dimensional chain. One spin-up electron and one spin-down electron are deployed on the first and second site, each. Initially, there are no correlations.

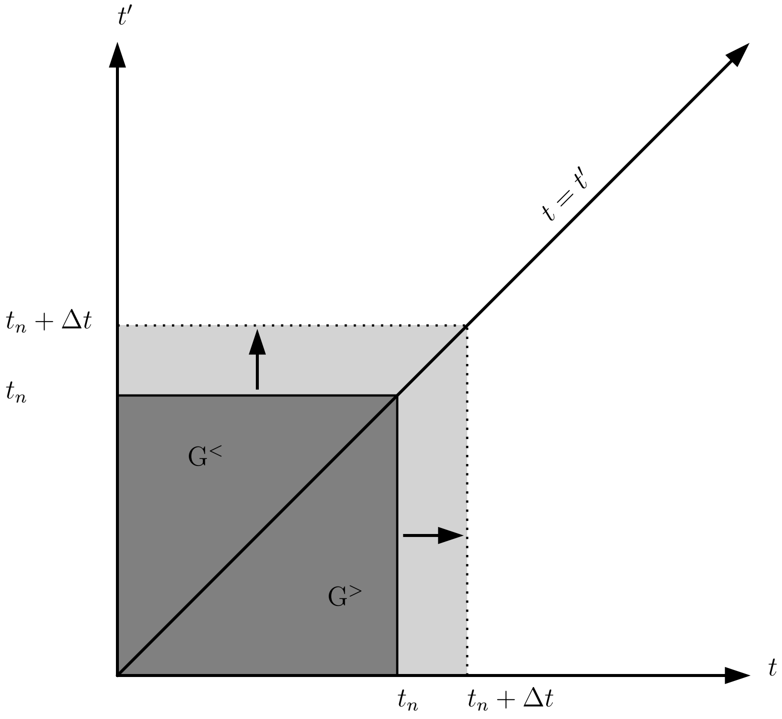

Figure 3.3: Illustration of the time propagation on the two-dimensional time plane.

4 Quantitative Analysis

4.1 The Time Reversal Switch Function

The first approach was to accomplish time reversal by simply reversing the sign of the Hamiltonian, that is by multiplying the Hamiltonian with a step function that returns plus one before and minus one after the return time t_{tr}. That was not successful, however. Figure 4.1 shows the density evolution on each of the four sites during a simulation where time reversal occurs at $t = 10$. The sample rate r_{sample} is a parameter that increases numerical accuracy when decreased, similar to the time step[1]. The system clearly does not return into its initial state, although an increase in numerical accuracy does somewhat ease the problem. It turns out, however, that this is not simply a problem of numerical accuracy. Figure 4.2 shows the energy evolution during the first of the two simulations shown in Fig. 4.1. The oscillations seen in panel (a) are typical of numerical problems. In this case the problem lies with the fact that the Hamiltonian was non-continuous during time reversal. Since the time-stepping algorithm uses multiple previous time steps in the calculation of the next time step, shortly after time reversal, it uses energies from before time reversal that differ from the energies after time reversal by $2U$. In the case of a continuous Hamiltonian, that difference could (in theory) become arbitrarily small for arbitrarily small time steps. Fortunately, the above analysis is valid for a wide range of Hamiltonians, including time-dependent ones. Therefore it is possible to substitute the simple, non-continuous step function by a more complicated, but still antisymmetric function f_{trsf} that is defined by

$$f_{\text{trsf}}(t) = \\ \begin{cases} 1, & \text{for} \quad t < t_{\text{tr}} - \tau \\ -\frac{3}{8}\left(\frac{t-t_{\text{tr}}}{\tau}\right)^5 + \frac{10}{8}\left(\frac{t-t_{\text{tr}}}{\tau}\right)^3 - \frac{15}{8}\left(\frac{t-t_{\text{tr}}}{\tau}\right), & \text{for} \quad t_{\text{tr}} - \tau \leq t \leq t_{\text{tr}} + \tau \\ -1, & \text{for} \quad t_{\text{tr}} + \tau \leq t \end{cases} \tag{4.1}$$

where τ is a parameter describing the width of the switching. This function, as well as its first and second derivative, is continuous. It is also antisymmetric with respect to t_{tr}. The time reversal switch function is illustrated in Fig. 4.3.

---

[1] The algorithm that is used for time propagation is a point sampling scheme, which means that for the integration in the calculation of the next step, only every r_{sample}-th point is used. Doing this while increasing the order of the propagation scheme proves to be more efficient for a given numerical effort than using a simple scheme that is more accurate in the calculation of the integral, but of lower order.

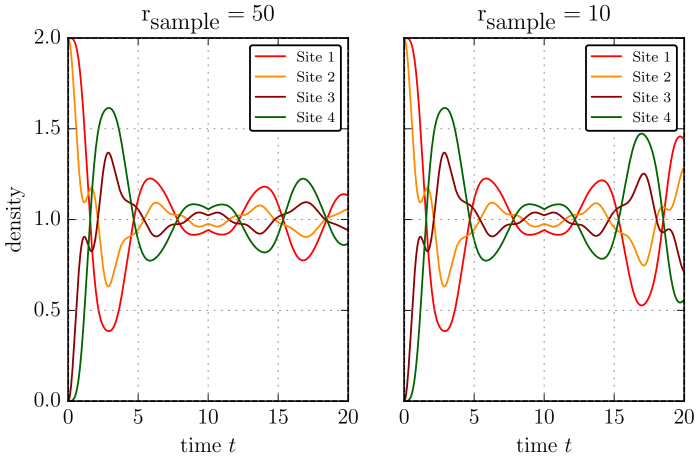

Figure 4.1: Time-reversed simulation of a one-dimensional four-site Hubbard chain in TPP. Time-reversal occured at t = 10. The interaction strength was $U = 1$.

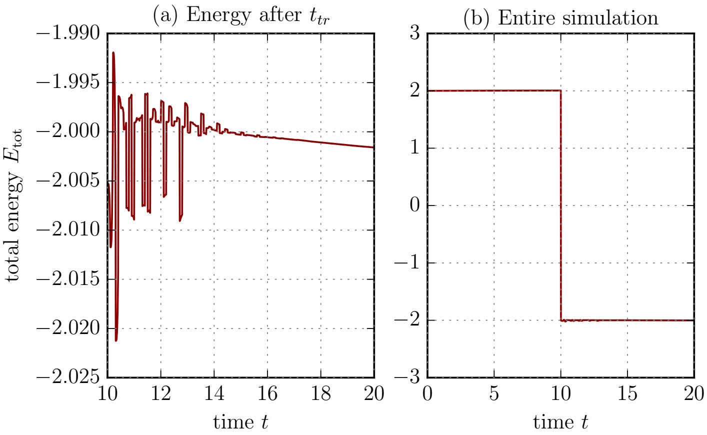

Figure 4.2: Time-reversed TPP simulation of a one-dimensional four-site Hubbard chain. Shown is the total energy (a) during the entire simulation and (b) after time reversal. For the paramters, see Fig. 4.1

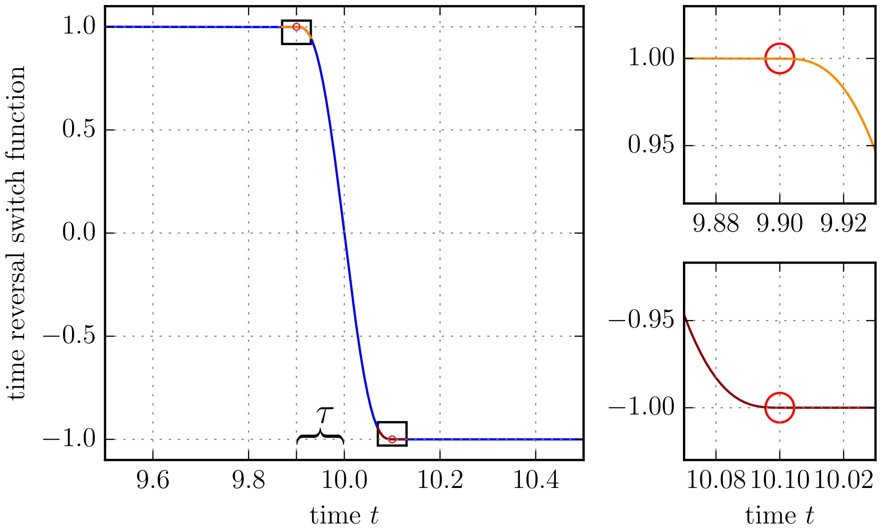

Figure 4.3: Illustration of f_{trsf} with $\tau_{\mathrm{tr}} = 0.1$. The points where the piecewise defined parts of the function are joined are drawn more closely on the right hand side of the figure, and marked by red circles.

In th following analysis, unless otherwise specified, the time reversal switching width has been chosen to be $\tau_{\mathrm{tr}} = 0.3$.

4.2 Reversed and Perturbed TPP Simulations

With the continuous time reversal switch function the numerical problems responsible for the damping of the reversed calculation in Fig. 4.1 disappear. Figure 4.4 shows the results of a time reversed TPP simulation. The time evolution of the entanglement entropy is shown for exact reversal, i.e., $\Delta U = 0$ as well as for slightly perturbed systems. On panel (b), the backwards calculated entropy has been projected onto physical time. The interaction strength is $U = 1$. It can be seen that even for a relatively large perturbation $\Delta U = 0.1$, which is 10% of the total interaction strength, the backward calculation does not deviate too far from the forward calculation. This is partly due to the very small size of the system. However, it might be interesting to see how the quality, or stability, of time reversal depends on different parameters, such as the propagation time or the interaction strength, and of course, of the method used to calculate the simulation.

It is therefore useful to define a quantity q that measures how well a system returns into its inital state. This quantity can then be compared for various values of the aforementioned parameters. One possibility is to calulate the mean squared difference of the backward from the forward calculation for a given

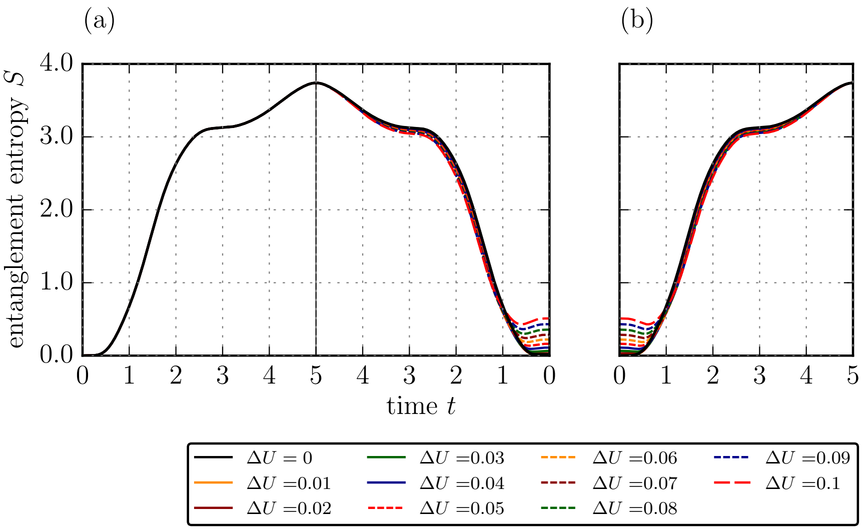

Figure 4.4: Time evolution of the entanglement entropy in time reversed, perturbed TPP simulations. Panel (b) shows essentially the same as panel (a), except for the fact that the part after the time reversal (at $t = 5$) has been projected onto physical time, so as to better compare it with the forward calculated part (in black). The interaction strength is $U = 1$.

parameter p:

$$q(p) = \sqrt{t_{\mathrm{tr}}}\,\frac{\sqrt{\displaystyle\int_0^{t_{\mathrm{tr}}} \mathrm{d}t\,\Big[p(t) - p(t_{\mathrm{tr}} - t)\Big]^2}}{\displaystyle\int_0^{t_{\mathrm{tr}}} \mathrm{d}t\,p(t)}\,. \tag{4.2}$$

Figure 4.5 shows one example of that. The deviation q has been calculated for the entanglement entropy S, the correlation energy E_{corr}, the kinetic energy E_{kin}, the Hartree–Fock energy E_{HF} and the densities on all four sites (shown here is the average of these four deviations). For comparison, the actual time evolution of these parameters is also shown in the smaller panels. For the Hartree–Fock energy, the kinetic energy and the densities, the deviation grows linearly with the perturbation ΔU, while the correlation energy as well as the entanglement entropy deviations seem to grow quadratically with ΔU. Of all the parameters that have been considered, the density deviates the least from the initial state. The correlation energy and Hartree–Fock energy deviate the most. The reason for that is that they depend depend explicitly on U, cf. Eqs. (2.51) and (2.52). This can be seen in the small right-hand panels of Fig. 4.5. Close to the point of time reversal (within a margin of τ_{tr}, to be precise), most of the behaviour of all the energies is governed by the influence of the time reversal switch function. The Hartree–Fock and correlation energies evolve qualitatively very similar for all perturbations, but they are shifted by a near constant value. This is due to their U-dependence and can be understood when considering

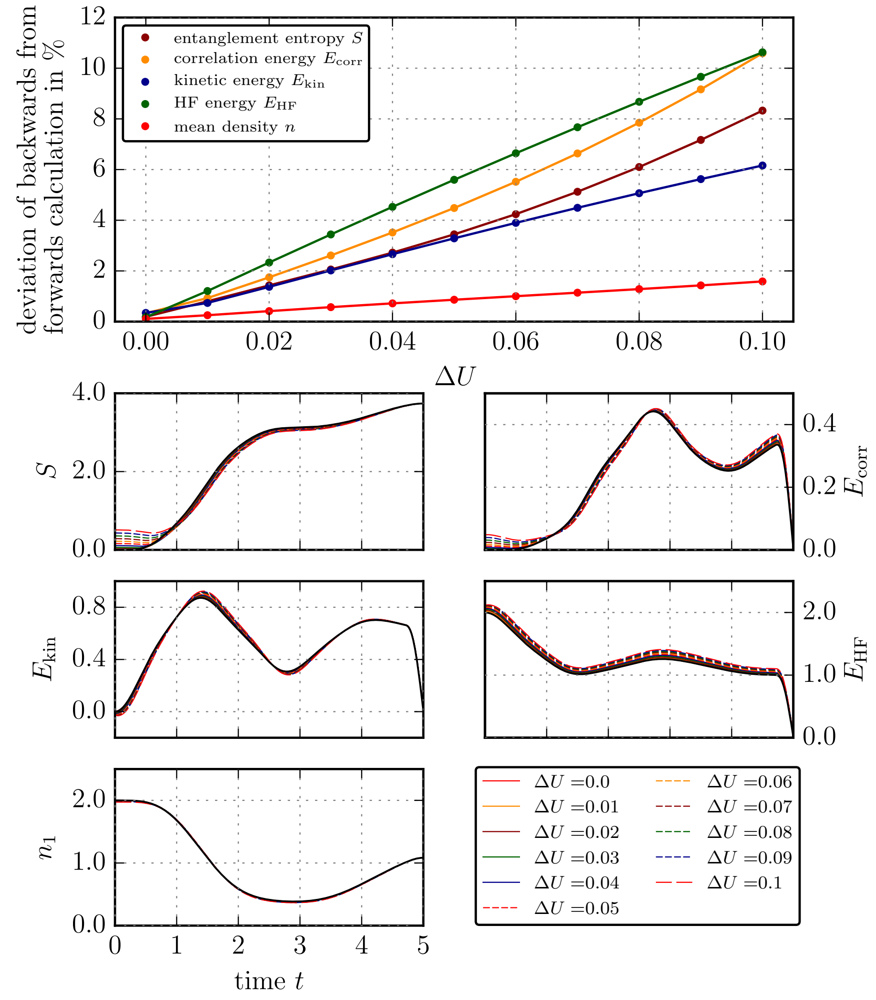

Figure 4.5: Mean square deviation of forwards calculated quantities from backwards calculated quantities in TPP simulations. The smaller frames show the direct comparison. 'Mean density' indicates the mean deviation of the four densities. (The mean density is always constant due to particle number conservation, therefore its deviation will always be zero.) The interaction strength is $U = 1$.

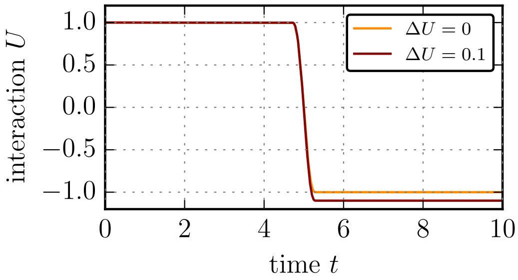

Figure 4.6: The influence of the perturbation ΔU on the interaction strength U.

the influence of ΔU on U. This influence is illustrated in Fig. 4.6. The time dependence of U can be written as

$$U(t) = f_{\mathrm{trsw}}(t) \begin{cases} U & t < t_{\mathrm{tr}} \ , \\ U + \Delta U & t > t_{\mathrm{tr}} \ . \end{cases} \tag{4.3}$$

Note that even for $\Delta U \neq 0$, the interaction strength is still continuous, though no longer differentiable in $t = t_{\mathrm{tr}}$, since $f_{\mathrm{trsw}}(t_{\mathrm{tr}}) = 0$. This behaviour is very similar to the one displayed by the U-dependent energies in Fig. 4.5.

4.2.1 Effect of the Interaction Strength U on Time Reversal Quality Q

Since both the Hartree–Fock energy and the correlation energy depend explicitly on U, after time reversal, they depend explicitely on ΔU as well. Thus, let the parameter Q that describes the time reversal quality of a simulation be the average of the deviations of those quantities that do not depend on U:

$$Q = \frac{1}{3}\Big[q(S) + q(E_{\mathrm{kin}}) + q(n)\Big] \ . \tag{4.4}$$

Figure 4.7 shows the dependence of the time reversal quality on the interaction strength. The most striking feature of the figure is the fact that the deviations are very large for weakly interacting systems with $U = 0.1$ (except for the densities). To understand this, it is useful to look at the dependence of all these quantities on the interaction strength. The kinetic energy and the entanglement entropy do not explicitely depend on U, but the entanglement entropy in particular is a measure of the correlation of the system, which obviously depends on the interaction.

Figure 4.8 shows that the entanglement entropy converges after some time towards some (U-independent) value. The rate of the convergence, however, depends heavily on U and in particular, it is very slow for small U. It converges to some constant rate at around $U = 1$. This explains why for small U, a comparatively small perturbation ΔU can have considerable effects.
For larger interaction strengths, the quality of time reversal decreases with increasing U, and the dependence on ΔU seems to become nonlinear.

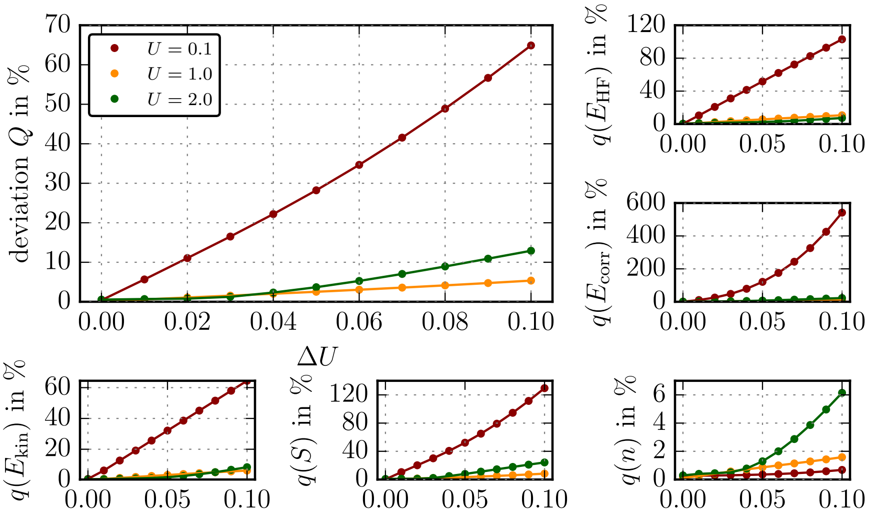

Figure 4.7: Mean square deviation of forwards calculated quantities from backwards calculated quantities in TPP simulations for different interaction strengths U and different perturbations ΔU. The smaller frames show deviations for single quantities. The return time is $t_{\mathrm{tr}} = 5$.

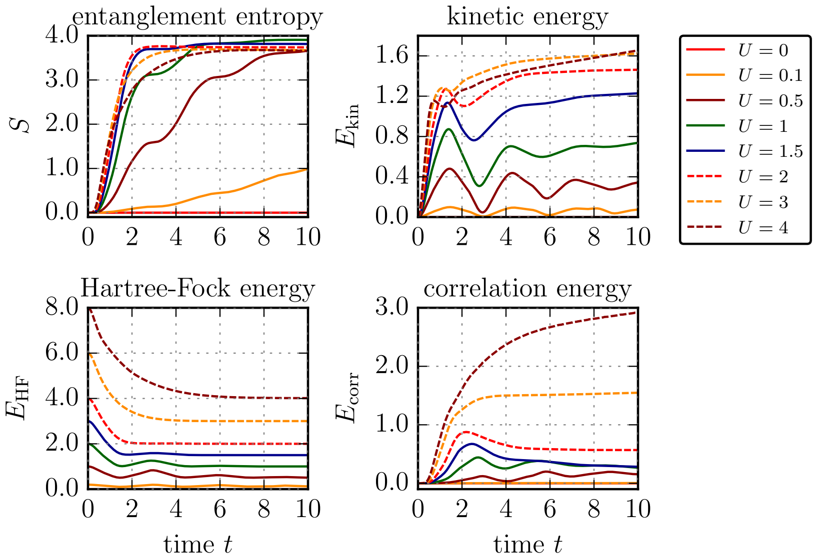

Figure 4.8: Time evolution of different parameters in (non-reversed) TPP simulations for different interaction strengths U.

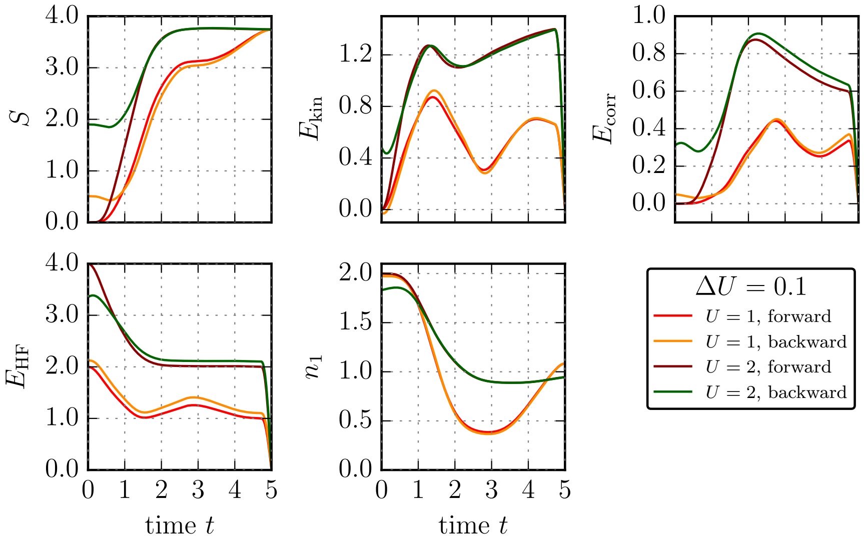

Figure 4.9: Influence of interaction strength on time reversibility of perturbed TPP simulations. The return time is $t_{\mathrm{tr}} = 5$.

Figure 4.9 shows a possible (qualitative) reason for that behaviour. For larger interaction strengths, the system shows the damped behaviour described earlier, in section 2.2.5. This is particularly clear for the entanglement entropy and the density. The entropy reaches its final value at around $t = 2$, and the density (on site 1) at around $t = 3$. In a sense, the converged values occupy a much denser part of the parameter space, since the probability of the system to have reached these values becomes very high after some time. Therefore it is to be expected that time reversal is less stable once the converged state has been reached.

For GKBA+TPP simulations (Fig. 4.10) and exact diagonalization simulations (Fig. 4.11) the tendencies are very similar, with the notable exception that for large U the time reversal quality does not seem to depend very much on U, and the nonlinear dependence of q of ΔU disappears. This is further evidence that this behaviour was due to the unphysical damping of the full TPP simulation. The damping effects become much more obvious at very large perturbations.
This can be seen in Fig. 4.12. The perturbations ΔU are of the order of magnitude of the interaction strength U. Still, particularly for the density, the system does not deviate entirely from the forward calculation, especially in the beginning. For such large perturbations, the mean square deviations q increase less with increasing ΔU than they did for smaller ΔU. The entanglement entropy and density deviations, as well as the kinetic energy deviations, tend to some saturated value. This is due to two main reasons.
Firstly, the parameter space for this very small, very simple system consisting

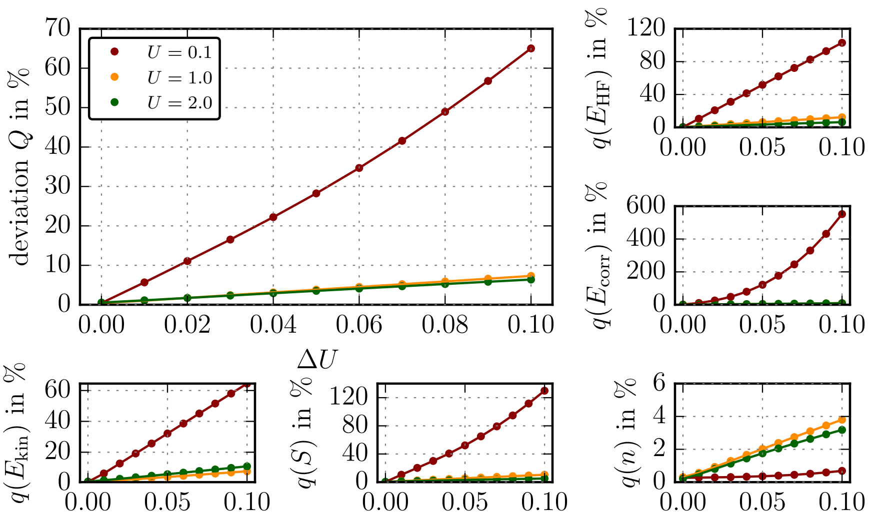

Figure 4.10: Mean square deviation of forwards calculated quantities from backwards calculated quantities in GKBA+TPP simulations for different interaction strengths U and different perturbations ΔU. The smaller frames show deviations for single quantities. The return time is $t_{\mathrm{tr}} = 5$.

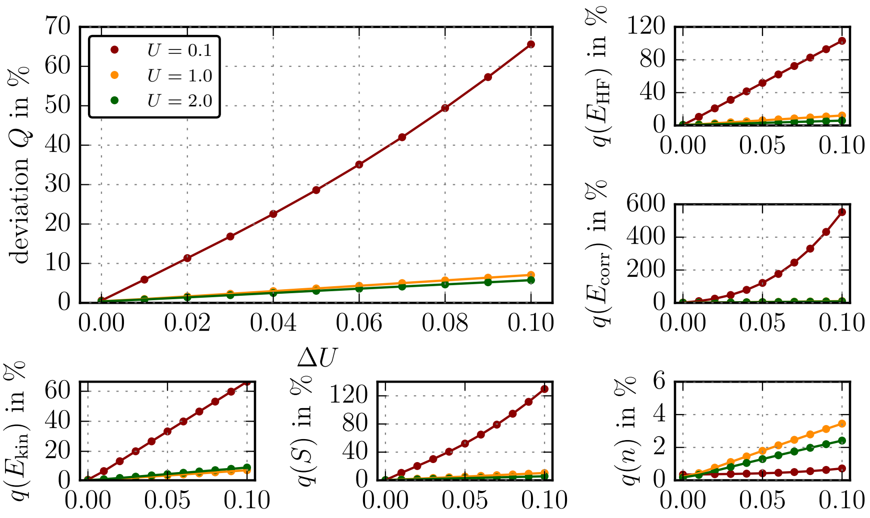

Figure 4.11: Mean square deviation of forwards calculated quantities from backwards calculated quantities in exact diagonalization for different interaction strengths U and different perturbations ΔU. The smaller frames show deviations for single quantities. The return time is $t_{\mathrm{tr}} = 5$.

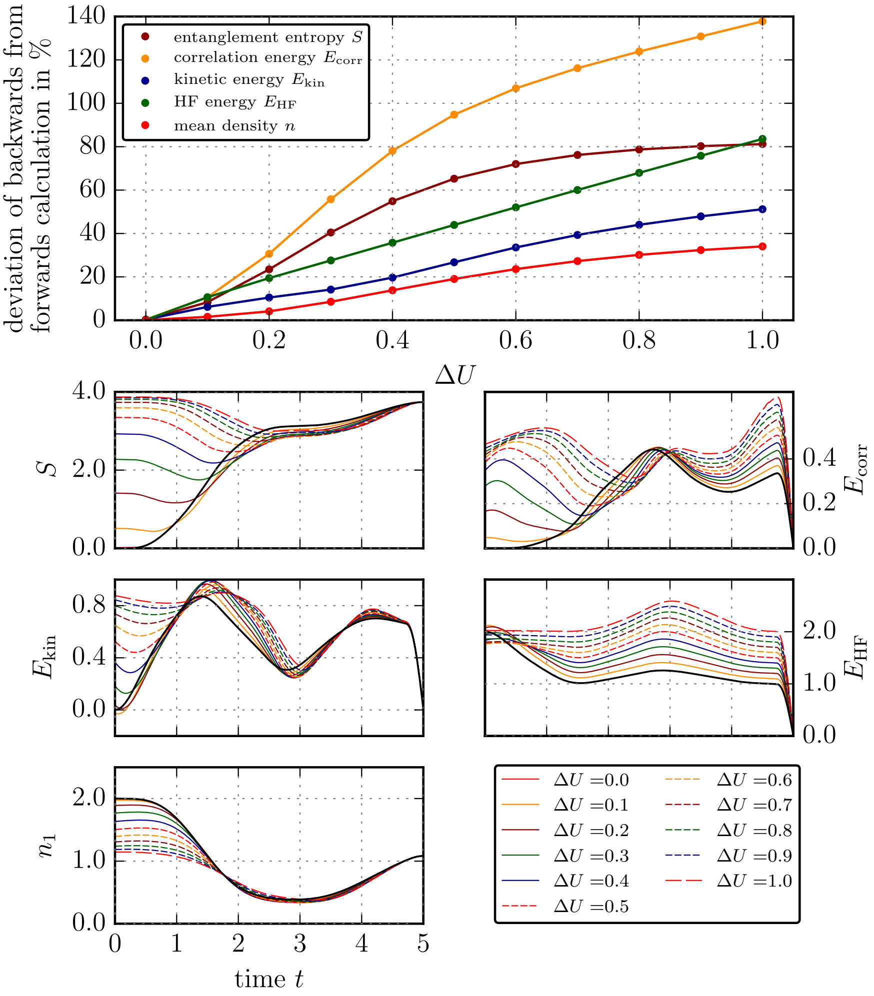

Figure 4.12: Mean square deviation of forwards calculated quantities from backwards calculated quantities in TPP simulations. The smaller frames show the direct comparison. 'Mean density' indicates the mean deviation of the four densities. (The mean density is always constant due to particle number conservation, therefore its deviation will always be zero.) The interaction strength is $U = 1$.

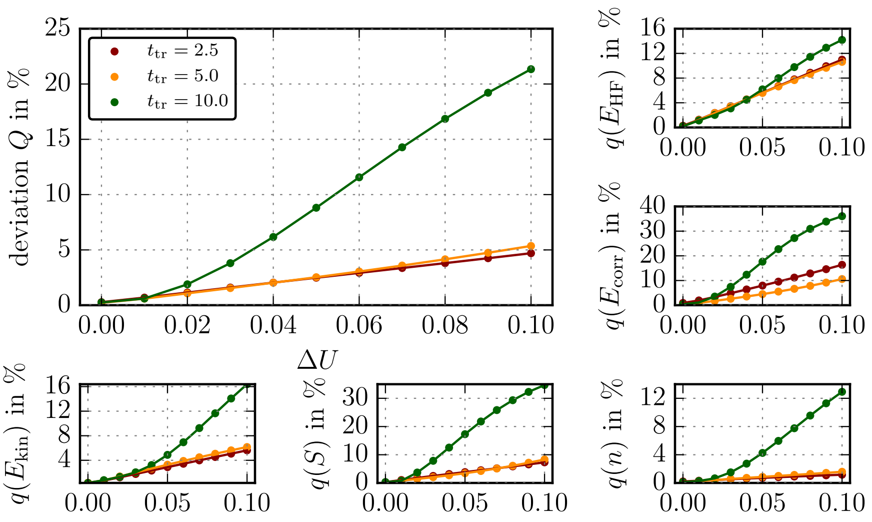

Figure 4.13: Mean square deviation of forwards calculated quantities from backwards calculated quantities in TPP simulations for different propagation durations and different perturbations ΔU. The smaller frames show deviations for single quantities. The interaction strength is $U = 1$.

only of four electrons and four atomic sites is limited and it is simply not possible to deviate arbitrarily far from any given path.
Secondly, if the system is very perturbed it will not return to its initial state at all, but rather tend to the damped steady state. The propagation will then not change very much for even higher ΔU. This is most obvious for the entanglement entropy. It can be seen in Fig. 4.12 that the evolution is very similar for $\Delta U = 0.9$ and $\Delta U = 1.0$. The correlation energy and the Hartree–Fock energy, on the other hand, depend explicitly on U, therefore the deviation will continue to grow with growing ΔU (i.e., growing U).

4.2.2 Effect of the Propagation Time on Time Reversal Quality Q

The influence of the propagation duration on the stability of time reversal seems straightforward on first sight, the longer the duration, the higher the deviation from the forward calculation for a given perturbation. For the exact diagonalization and for the GKBA calculation (Figs. 4.14 and 4.15) that is exactly the case.

For the TPP simulations (Fig. 4.13) it is not quite as simple, which, of course, is again due to the unphysical damping. In this case, the difference in deviations between $t_{\mathrm{tr}} = 2.5$ and $t_{\mathrm{tr}} = 5$ is small, and it even varies from parameter to parameter which one deviates more.
The deviation for $t_{\mathrm{tr}} = 10$ starts to converge towards a constant value for the entanglement entropy and the correlation energy, though that is not the case

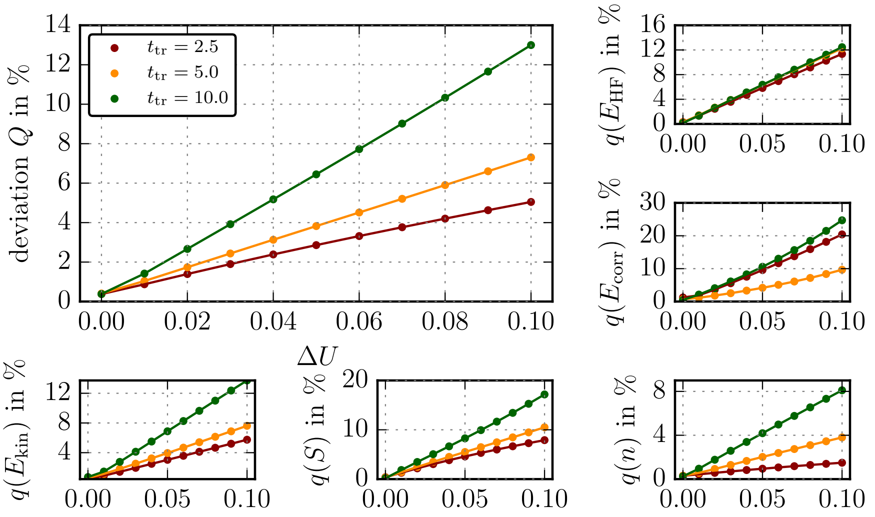

Figure 4.14: Mean square deviation of forwards calculated quantities from backwards calculated quantities in GKBA+TPP simulations for different propagation durations and different perturbations ΔU. The smaller frames show deviations for single quantities. The interaction strength is $U = 1$.

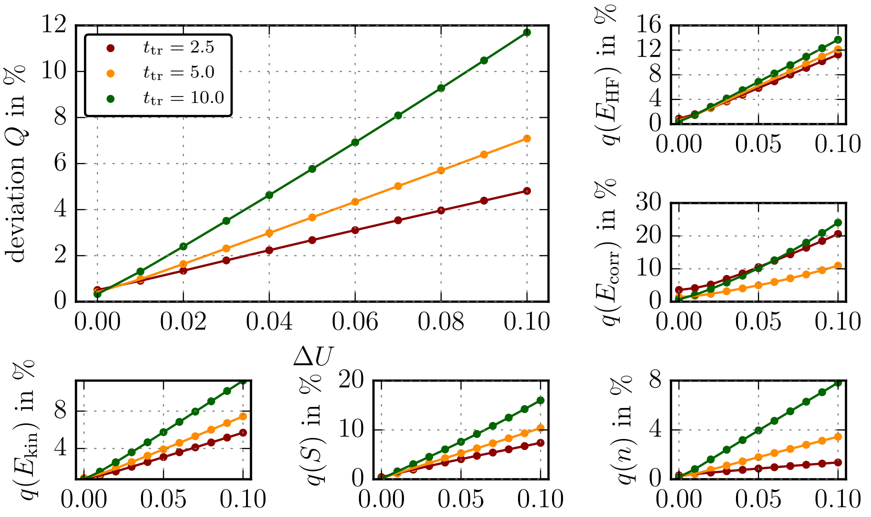

Figure 4.15: Mean square deviation of forwards calculated quantities from backwards calculated quantities in exact diagonalization for different propagation durations and different perturbations ΔU. The smaller frames show deviations for single quantities. The interaction strength is $U = 1$.

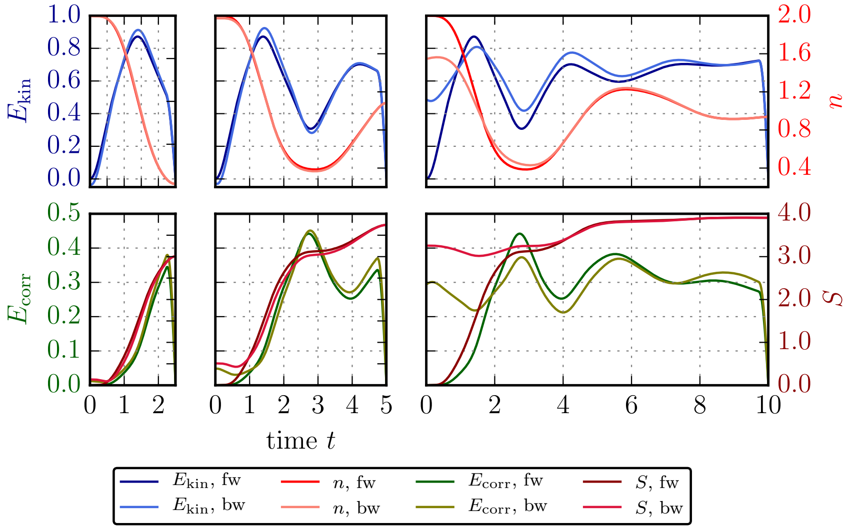

Figure 4.16: Time evolution of various quantities in time reversed TPP simulations for different propagation times. The interaction strength is $U = 1$, the perturbation of the interaction strength is $\Delta U = 0.1$.

either for the kinetic energy or for the density, whose deviations are, on the other hand, much smaller.

Figure 4.16 shows the time evolution (forwards and backwards calculated) of these quantities for $\Delta U = 0.1$ and for the three different propagation times. The entanglement entropy in particular does not deviate very far from the entirely damped state for $t_{\mathrm{tr}} = 10$. The entanglement entropy, in general, is always zero in the initial state (the system is uncorrelated in the beginning) and converges to some constant non-zero value later on (at least, that is what happens in the TPP simulations).
If it does not return into the initial state, then the deviation is necessarily large. Similar things are true for the correlation energy, which is also a measure of the correlation of the system: It starts out at zero and converges later on. Additionally, the correlation energy depends explicitely on U.

4.3 Summary

One thing that all simulations, for all interaction strengths, propagation durations and approximations, have in common, is that they are indeed exactly time reversible for $\Delta U = 0$. The time reversal properties of GKBA simulations are more similar to those of the exact diagonialization than those of TPP simulations are. This is mostly due to the unphysical damping observed in the full method.
The influence of the interaction strength U on the quality of time reversal is

complex, and deserves further analysis. The dependency of the behaviour of the system on U depends itself on U. It seems that the system is far more sensitive to perturbations in U for small U.

Longer propagation times lessen the quality of time reversal. The exact relation depends on the simulation method.

In general the choice of ΔU as a perturbation parameter should be critically assessed. The interaction strength has many obvious and some more subtle influences on the behaviour of a system. Particularly if one is interested in potential chaotic behaviour of larger systems it might be difficult to separate the effects that stem from the direct influence of the interaction strength from the stability of the system. At least it might be interesting to see whether the perturbation of different parameters has similar effects on the time reversibility of the system.

5 Conclusion and Outlook

In this thesis it has been shown that the governing equations of the Green functions theory, which are the Martin–Schwinger hierarchy and the Kadanoff–Baym equations, are analytically exactly time reversal invariant, and that reversing time is formally equivalent to reversing the sign of the Hamiltonian. The same holds true for all the approximations to the selfenergy that have been treated in this thesis, which are the Hartree–Fock selfenergy, the second Born selfenergy and the T-matrix selfenergy.

For small systems, the numerical time reversal is quite stable with respect to small perturbations of the Hamiltonian, as long as that Hamiltonian is sufficiently continuous. Simulations done with the generalized Kadanoff–Baym ansatz display similar behaviour with respect to time reversal as exact diagonalization does. The full two-times simulations, on the other hand, behave in some instances differently due to the unphysical damping that is characteristic to those methods.

Amongst the next possible steps there is the analysis of time reversal invariance of the generalized Kadanoff–Baym ansatz and a theoretical treatment of the influence of ΔU by a perturbative approach.
On the numerical side, it could be interesting to consider the influence of both the size and particle number as well as the dimension of the system on the quality of time reversal. Another possibility would be to perturb some other parameter rather than the interaction strength and to compare in particular the dependence of the time reversibility quality for varying ΔU of the interaction strength.
In conclusion, the use of time reversal symmetry in numerical testing is justified for the nonequilibrium Green functions formalism, since the equations are exactly time reversible and since that reversibility is sufficiently stable not to be influenced by the inherently limited accuracy of computers.

Bibliography

[1] H. Wegener and G. Ischenko. Symmetriebetrachtungen in der modernen physik. das pct-theorem. *Erlanger Forschungen, Reihe B*, 3, 1968.

[2] B. Werner P. Vogel. Final-state interactions and time-reversal tests in nuclear β-decay. *Nucl. Phys. A*, 404, 1983.

[3] M. Schwartz. *Quantum Field Theory and the Standard Model*. Cambridge University Press, 2014.

[4] J. P. Lees et al. Observation of time-reversal violation in the B^0 meson system. *Phys. Rev. Lett.*, 109:211801, 2012.

[5] M. Puig von Friesen, C. Verdozzi, and C.-O. Almbladh. Kadanoff-baym dynamics of hubbard clusters: Performance of many-body schemes, correlation-induced damping and multiple steady and quasi-steady states. *Phys. Rev. B*, 82:155108, 2010.

[6] A. Stan. On the unphysical solutions of the kadanoff–baym equations in linear response: Correlation-induced homogeneous density-distributions and attractors. *Phys. Rev. B*, 93:041104, 2016.

[7] F. Brito, F. Rouxinol, M. D. LaHaye, and A. O. Caldeira. Testing time reversal symmetry in artificial atoms. *New J. Phys.*, 17(7):075002, 2015.

[8] M. Bonitz. *Quantum Kinetic Theory*, volume 33 of *Teubner-Texte zur Physik*. B. G. Teubner, 1998.

[9] M. Bonitz and D. Semkat. *Introduction to Computational Methods in Many Body Physics*. Rinton Press, 2006.

[10] K. Balzer and M. Bonitz. *Nonequilibrium Green's Functions Approach to Inhomogeneous Systems*, volume 867 of *Lecture Notes in Physics*. Springer-Verlag, 2013.

[11] N. Schlünzen, S. Hermanns, M. Bonitz, and C. Verdozzi. Dynamics of strongly correlated fermions: Ab initio results for two and three dimensions. *Phys. Rev. B*, 93:035107, 2016.

[12] D. Hochstuhl, K. Balzer, S. Bauch, and M. Bonitz. Nonequilibrium green functions approach to photoionization processes in atoms. *Phys. E*, 42(3):513, 2010.

[13] S. Hermanns. *Nonequilibrium Green Functions approach to Hubbard nanoclusters using the generalized Kadanoff-Baym ansatz.* Diploma thesis, University of Kiel, 2012.

[14] K. Balzer, M. Bonitz, R. van Leeuwen, A. Stan, and N. Dahlen. Nonequilibrium green functions approach to strongly correlated few-electron quantum dots. *Phys. Rev. B*, 79:245306, 2009.

[15] N. Schlünzen and M. Bonitz. Nonequilibrium green functions approach to strongly correlated fermions in lattice systems. *Contrib. Plasma Phys.*, 56:5, 2016.

[16] H. Tasaki. The hubbard model – an introduction and selected rigorous results. *J. Phys. Condens. Matter*, 10:4353, 1998.

[17] N. Schlünzen. *Nonequilibrium Green functions analysis of electron dynamics in strongly correlated lattice systems.* Master thesis, University of Kiel, 2015.

[18] P. Lipavský, V. Špička, and B. Velický. Generalized kadanoff-baym ansatz for deriving quantum transport equations. *Phys. Rev. B*, 34:6933, 1986.

[19] F. Haake. *Quantum Signatures of Chaos.* Springer-Verlag, 2001.

Erklärung

Ich erkläre hiermit, dass ich die vorliegende Arbeit selbstständig und ohne unerlaubte fremde Hilfe angefertigt habe, andere als die angegebenen Quellen und Hilfsmittel nicht benutzt habe, die den benutzten Quellen wörtlich oder inhaltlich entnommenen Stellen als solche kenntlich gemacht und die vorliegende Arbeit nicht an anderer Stelle eingereicht habe. Die digitale Version entspricht dem Stand der schriftlichen Fassung.

Kiel, den ____________________ ____________________________
Miriam Scharnke